DOKUZ EYLÜL UNIVERSITY
GRADUATE SCHOOL OF NATURAL AND APPLIED SCIENCES

MODELING OF STRAIN-ELECTRICAL RESISTANCE RELATION OF SMART CONCRETE

by
Aurore MUGISHA

February, 2018
İZMİR

MODELING OF STRAIN-ELECTRICAL RESISTANCE RELATION OF SMART CONCRETE

A Thesis Submitted to the
Graduate School of Natural and Applied Sciences of Dokuz Eylül University
In Partial Fulfillment of the Requirements for the Degree of
Master of Science in Civil Engineering, Structural Engineering Program

by

Aurore MUGISHA

February, 2018
İZMİR

M.SC. THESIS EXAMINATION RESULT FORM

We have read the thesis entitled **"MODELING OF STRAIN-ELECTRICAL RESISTANCE RELATION OF SMART CONCRETE"** completed by **AURORE MUGISHA** under supervision of **ASSOC. PROF. DR. EGEMEN TEOMETE** and we certify that in our opinion it is fully adequate, in scope and in quality, as a thesis for the degree of Master of Science.

.....

Assoc. Prof. Dr. Egemen Teomete

Supervisor

.....

Prof. Dr. Yıldırım ERTÜTAK

(Jury Member)

.....

Yrd. Doç. Dr. Mutlu SEGER

(Jury Member)

.....

Prof. Dr. Kadriye ERTEKİN

Director

Graduate School of Natural and Applied Sciences

ACKNOWLEDGEMENT

I would like to express my sincere gratitude to my advisor Assoc. Prof. Dr. Egemen Teomete whose thoughtful guidance and critical comments helped me in all the time of the research.

I would also like to thank Prof. Dr. Kambiz Ramyar from the Civil Engineering Department at Ege University for his academic and moral support during my studies in Turkey as an undergraduate and graduate student.

I acknowledge Res. Asst. Mehmet Uyar from the department of Mechanical Engineering at Dokuz Eylül University, whose suggestions and comments on modeling using ANSYS program were eye-opening.

I would like to thank TUBITAK for supporting the project "Smart Concrete Production " (project number 213M452).

I warmly thank and appreciate my family for their unconditional support, especially my beloved fiancé Guylain whose great patience encouraged me during the tough times and enabled me to complete this work.

Finally I thank God, my good Father, for the divine inspiration throughout my research and the grace of achieving my degree.

Aurore MUGISHA

MODELING OF STRAIN-ELECTRICAL RESISTANCE RELATION OF SMART CONCRETE

ABSTRACT

The performance of infrastructures is adversely affected by natural disasters, material degradations and other environmental factors. Structural health monitoring is an important issue regarding the safety of lives and asset management. The metal strain gages which are widely used in structural health monitoring are not durable, are costly and have low sensitivity. In this thesis, numerical models were developed for the piezoresistive behavior of smart concrete based on finite element method. Finite element models were designed using experimental data collected from compression test. The compression test was performed on smart concrete cube specimens with 75mm dimensions. Smart concrete was made of cement CEM II 42.5 R, silica fume, fine and coarse crushed limestone aggregates, brass fibers and plasticizer. During the compression test, electrical resistance change and compressive strain measurements were conducted simultaneously. Smart concrete had a strong linear relationship between strain and electrical resistance change. This relation is called piezoresistivity. These experimental observations were modeled by numerical methods. Twenty-noded solid brick elements SOLID226 were used to model the smart concrete specimens in the finite element platform of ANSYS Multiphysics 14.0. The numerical results were determined for strain induced resistivity change. The electrical resistivity of simulated smart concrete decreased with applied strain, as found in experimental investigation. The numerical findings are in good agreement with the experimental results. Modeling of smart concrete will enable the creation of a model that can be used by structural engineers.

Keywords: Finite element model, smart concrete, electrical resistivity change, piezoresistivity, structural health monitoring

AKILLI BETONUN BİRİM ŞEKİL DEĞİŞTİRMESİ-ELEKTRİKSEL DİRENÇ İLİŞKİSİNİN MODELLENMESİ

ÖZ

Altyapıların performansı doğal afetler, malzeme bozulmaları ve diğer çevresel faktörlerden olumsuz etkilenmektedir. Yapı sağlığının gözlenmesi, can ve mal güvenliği açısından önemli bir konudur. Yapı sağlığını gözlemek için yaygın olarak kullanılan gerinim pulları, düşük dayanıklı, maliyetli ve düşük duyarlılığa sahiptirler. Bu tezde, sonlu elemanlar metodu kullanılarak akıllı betonun piezorezistif davranışı için sayısal modeller geliştirilmiştir. Sonlu elemanlar modeli, akıllı beton üzerinde yapılan basınç testinden toplanan deneysel veriler kullanılarak tasarlanmıştır. Basınç testi 75 mm boyutlu akıllı beton küp numuneleri üzerinde yapılmıştır. Akıllı beton çimento CEM II 42.5 R, silika dumanı, kırma taş ince ve iri agregalar, pirinç lif ve akışkanlaştırıcıdan oluşturulmuştur. Basınç deneyi sırasında elektriksel direnç değişimi ve birim sekil değiştirme ölçümleri eş zamanlı olarak yapıldı. Akıllı betonun elektriksel direnç değişimi ile birim şekil değiştirmesi arasında güçlü doğrusal ilişki tespit edildi. Bu etkiye piezorezistive etki denir. Bu deneysel gözlemler sayısal yöntemler ile modellendi. ANSYS Multiphysics 14.0 sonlu elemanlar platformu kullanarak akıllı betonun numuneleri modellenmesi için 3 boyutlu SOLID226 elemanlar kullanılmıştır. Sayısal sonuçlar, birim şekil değiştirme etkisi altındaki özdirenç değişimi olarak tayin edildi. Simüle edilmiş akıllı betonun elektrik özdirenci, deneysel araştırmada da tespit edildiği gibi uygulanan birim şekil değiştirme ile azalmaktadır. Sayısal bulgular, deneysel sonuçları ile oldukça uyumludur. Akıllı betonun modellenmesi, yapı mühendisleri tarafından kullanılabilecek bir modelin oluşturulmasını sağlayacaktır.

Anahtar Kelimeler: Sonlu elemanlar modeli, akıllı beton, elektriksel özdirenç değişimi, piezorezistive etki, yapı sağlığının gözlenmesi

CONTENTS

Page

LIST OF FIGURES

Page

LIST OF TABLES

Page

CHAPTER ONE
INTRODUCTION

1.1 Literature Review

The structural condition or health of concrete structures during service life can be monitored considering various parameters including strain (or deformation), stress (or force), crack, damage, temperature and humidity. Structural health monitoring systems gradually become a technique deployed to faithfully and continuously assess the performance of concrete structures and to program maintenance and repair work in a more economical way. The conventional metal foil strain gages used for structural health monitoring can get pointwise measurement. Consequently, they have to be used in a wide range. They are more expensive, less durable and more restricted in sensitivity than cement based composites (Chung, 2002).

A new concept of smart or self-sensing mortar has been introduced. It involves the ability of mortar to sense its own strain due to the effect of strain on the electrical resistivity (Chen & Chung, 1993; Fu, Chung, Ma, & Anderson, 1997; Wen & Chung, 2000). This electromechanical phenomenon is called piezoresistivity; it is achieved by mixing electrically conductive fillers such as steel fiber, short carbon fiber, carbon nanotube (CNT) and nickel powder into conventional mortar. It takes its origin from the slight fiber pull-out upon microcrack opening and the consequent loosening in fiber-matrix interface (Chung, 2001; Wen & Chung, 2006). It enables the use of electrical resistance measurement to detect the strain of cement composites.

The inclusion of carbon fibers to cement composites decreases its electrical resistance and application of loads affects electrical resistance (Chung, 1998; Fu & Chung, 1997; Fu et al., 1997; Teomete & Erdem, 2011; Teomete & Koçyiğit, 2015). Strain sensitivity of steel fiber reinforced cement matrix composites was assessed in the literature. Strain was found to be strongly correlated with electrical resistance through crosstalk compression test (Teomete, 2014) and split tensile test (Teomete & Koçyiğit, 2013).

Several researchers studied the piezoresistive behavior of cement based materials. Xiao, Li & Ou (2010) proposed a piezoresistive model based on tunnel effect theory which can predict the strain-sensing property of carbon black filled cement based composite (CCBC) under complex loading conditions. They observed that the proposed model is able to assess the resistance behavior and strain gauge factors of CCBC under various loading and environmental conditions.

Carbon nanotubes and carbon fiber reinforced cement based sensors were investigated for piezoresistive properties. The electrical resistivity of the sensor material was found to decrease both under monotonically and cyclically applied strain fields (Azhari & Banthia, 2012).

A micromechanics model was developed to predict the piezoresistive properties of carbon nanotube cement-based nanocomposites and numerical simulations were compared to experimental results (García-Macías, D'Alessandro, Castro-Triguero, & Ubertini, 2017). Their conclusions highlighted that the strain-sensing capabilities of the cement-based nanocomposites was due to strain-induced changes in the volume fraction, filler orientation and changes in the tunneling resistance.

The main governing parameters for successfully model steel fiber reinforced concrete for shear behaviour in a finite element platform were determined as Poisson's ratio, elastic modulus, stress-strain behaviour and tensile strength of concrete (Islam et al., 2014).

Chowdhury (2017) investigated and modeled the strain sensing capability of two matrices containing metallic inclusions: Portland cement matrix and iron-based carbonate binder matrix, subjected to three point bending test. Portland cement matrix contained four different iron replacement percentages by volume (10%, 20%, 30% and 40 %). The simulation was based on finite element analysis. The results showed that the experimental change in resistance comply with the simulated values. The resistivity increased with increasing load for both matrices and the strain sensing response increased with increase in iron percentage.

In order to perform a piezoresistive analysis, the finite element analysis program ANSYS defines three material properties for a piezoresistive material model: the electrical resistivity, the elastic coefficients and the piezoresistive matrix. The finite elements available for piezoresistive analysis are PLANE223, SOLID226 and SOLID227 (ANSYS).

1.2 Object and Scope

Teomete (2017) developed smart concrete which can sense its strain by testing strain sensitivities of different mixtures having different conductive fillers at different volume percents. The most sensitive mixture was selected as smart concrete. In this thesis, the piezoresistive behavior of smart concrete under compression test was numerically modeled. In the literature, the piezoresistive behavior of smart concrete was not numerically modeled. In this context, the relation of strain and electrical resistivity of smart concrete was simulated in ANSYS Multiphysics version 14.0 by using the ANSYS Parametric Design Language (APDL). Three numerical models have been developed by using the material properties of concrete adopted from experimental study conducted by Teomete (2017). Twenty-noded solid brick elements (SOLID226) are used to model the piezoresistive material. The numerical results are presented in terms of electrical resistivity change ($\%\ \rho$) versus strain. A good agreement between numerical predictions and experimental results was achieved, indicating the reliability of FE models for future problems on smart concrete.

1.3 Thesis Overview

Chapter 1 includes the literature review on smart mortar and modeling, as well as the object and scope of the thesis. In Chapter 2, the materials and methods used in the production of smart concrete, the compression test procedures of the reference study and the model generation in ANSYS are presented. The results of this study are compared with the experimental work results and discussed in Chapter 3. Chapter 4 provides the conclusions of the present study.

CHAPTER TWO
MATERIALS AND METHODS

2.1 Smart Concrete Mix Design

The materials used in the design of smart concrete, the methods related to the preparation of test specimens and the compression test procedures of the reference study are presented in this chapter. Experimental study was conducted by Teomete (2017).

2.1.1 Materials and Design

The smart concrete mixture used in the experimental study was made of cement CEM II B-M (L-W) 42.5R, fine and coarse crushed limestone aggregates, silica fume, polycarboxylate-based plasticizer and a dispersion of randomly oriented short brass fibers. The fibers had an average length of 1.5 mm and an average diameter of 0.5 mm. The ratio of brass fiber volume to total volume was 0.8%. The materials used in the mix after moisture adjustment in the aggregates are presented at Table 2.1.

Pure copper wire mesh with square opening of 5 mm and wire diameter of 600 μm was used as electrode because of its high electrical conductivity.

The maximum aggregate size was in the range of 15-16 mm. According to this, the concrete mix design was made based on TS 802 "DESIGN OF CONCRETE MIXES" standard. The following steps were implemented during concrete design.

- The target compressive strength for non-air entrained concrete was selected as 45 MPa.
- The water / cement ratio was chosen as 0.37 for non-air entrained concrete.
- The water content was found as 228 kg/m^3 for an amount of 8-10 cm concrete slump.

- Based on the maximum size of aggregate and climate conditions, the air content to be used in the design was estimated as 2.2%.
- Plasticizer / binder ratio was taken as 1%.
- Plasticizer / water reduction ratio was taken as 10%.
- Silica fume / binder ratio was taken as 10%.
- 40% of the total aggregate was coarse aggregate, whereas 60% was fine aggregate.

Table 2.1 The mass proportion of the materials used in $1m^3$ concrete mix (after adjustment for aggregate moisture) (Teomete, 2017)

Components	**Mass (kg) in $1m^3$ Concrete**
Brass fiber	70
Cement CEM II	499
Gravel 5-15 mm	539
Sand 0-5 mm	808
Silica fume	55
Water	205
Plasticizer	6

2.1.2 Preparation of Smart Concrete Specimens

Three cube specimens with sides of 7.5 cm were prepared. They were designated as Specimen 1, 2 and 3. 7.5 cm cube molds made of steel were designed and manufactured especially for the experimental work. On both sides of each mold, there were 2 mm wide and 46 mm long slots designed to allow the copper wire mesh electrodes to pass through the molds, as illustrated in Figure 2.1.

First, the aggregates, cement and silica fume were placed in a mixer in 3 times and mixed each time. The plasticizer and the water were subsequently mixed in a separate container, placed in the mixer in 3 times and mixed each time. The conductive brass fibers were finally added in the wet-mix concrete.

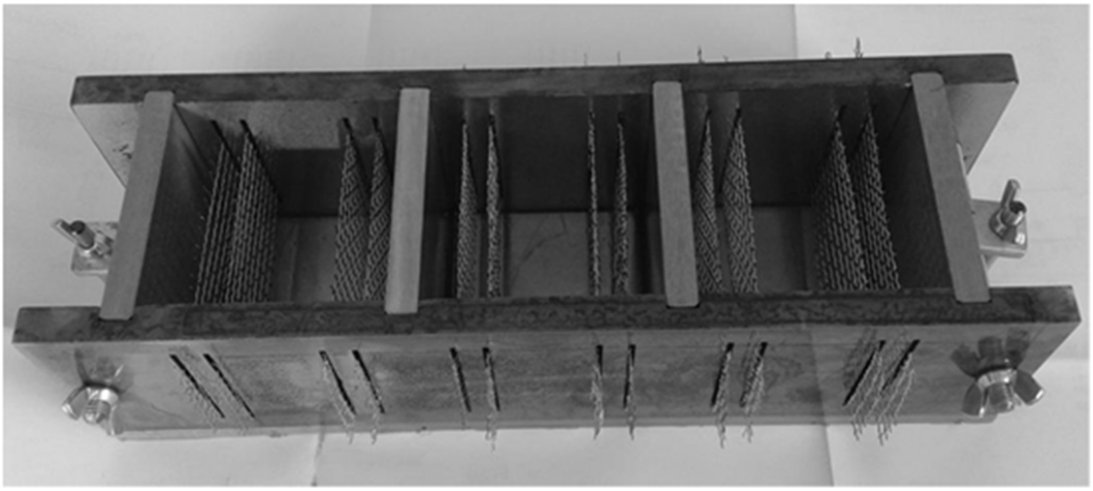

Figure 2.1 7.5 cm cube mold (Teomete, 2017)

The mixture was cast into the molds in 2 times. At each time, concrete was rod 10 times to avoid air bubbles. After the mix was cast, the mold was placed on a vibrating plate. After 24 hours, the specimens were demolded, cured for 28 days and kept at laboratory environment for 7 days in order to reach the steady state moisture content.

2.1.3 Compression Tests of Smart Concrete

Compression test was conducted in order to determine the electrical resistivity change (% ρ) - strain relationship of the specimens. Prior to loading, two strain gages were attached on every specimen to monitor the strain as seen in Figure 2.2 (a). Glass fiber epoxy composite plates were used to provide electrical insulation between the loading heads and the specimen as shown in Figure 2.2 (b). The test was performed with a displacement controlled Shimadzu mechanical test machine at a rate of 0.5 mm/min according to ASTM C39 standard.

Embedded four electrode method was used at the test. 20V DC current was supplied through one pair of outer electrodes (*Ec*), while the electrical potential difference across the sample (V_s) was measured using a different pair of inner electodes (E_v) as in Figure 2.2 (c). The sample was in series with a reference resistance R_r= 1000Ω. The potential difference across the reference resistance was

measured as V_r. The current I_m was measured during the test using a Digital Multimeter (DMM) which was in series with the circuit. The compressive strain and the electric current passing through the sample were parallel.

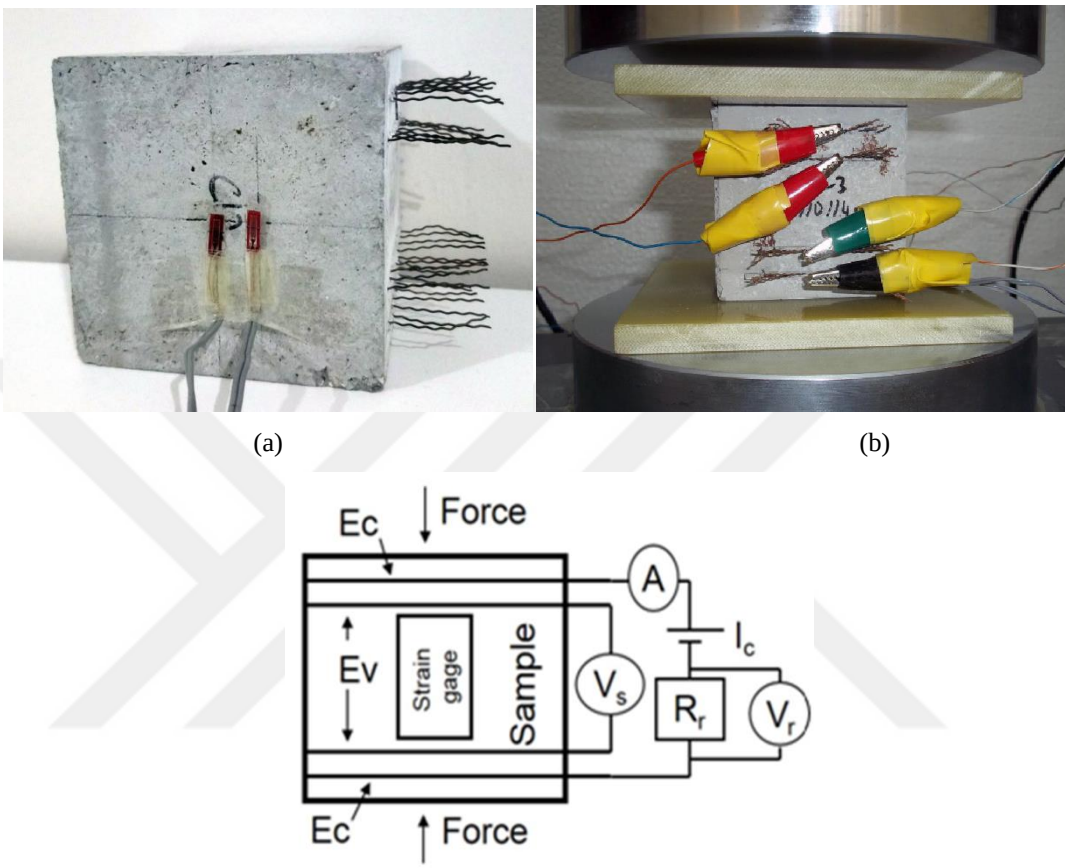

(a) (b)

(c)

Figure 2.2 Experimental setup during compression test (a) the prepared specimen (b) the specimen at test (c) the test circuit diagram (Teomete, 2017)

During the compression test, the strain gage data, the voltages (*Vs* and *Vr*), the electric current (I_m), the load and the stroke of the loading head were recorded at a rate of 10 Hz (10 data in a second) using a National Instruments data logger.

The electrical resistance of a sample (R_s) at any time of the test was determined by Ohm's Law as

$$R_s = \frac{V_s}{I_m} \tag{2.1}$$

The eletrical resistivity ρ and the percent change in the electrical resistivity of a specimen $\%\,\rho$ were respectively determined as

$$\rho = \frac{A}{L} \times R \tag{1.2}$$

$$\%\rho = \left(\frac{\rho}{\rho_o} - 1\right) \times 100 \tag{2.3}$$

where ρ_o is the electrical resistivity without any applied load, L the gage length, i.e. the length between the inner electrodes, and A is the cross-sectional area perpendicular to this length.

2.2 Model Development

2.2.1 Introduction

The compression tests conducted on the three specimens (Specimen 1, 2 and 3) were modeled numerically using finite element program ANSYS Multiphysics 14.0. To simulate the strain - electrical resistivity relation of smart concrete, three finite element models (FE-1, FE-2 and FE-3) were developed for the piezoresistive behavior of each smart concrete specimen. Piezoresistive static analysis was performed for each model.

2.2.2 Element Type Selection

The finite element models of the smart concrete specimens were constructed using SOLID226 elements. SOLID226 element has twenty nodes with up to five degrees of freedom (DOFs) per node. In the present work, four DOFs were used for

translations in the nodal x, y and z directions and voltage for electrical conduction field. This translates to the capability of the solid element to model problems involving both structural and electrical properties of smart concrete.

In this study, the numerical model of smart concrete was assumed to be isotropic, linearly elastic and free of voids. The elasticity capability of SOLID226 element is available to model the behavior of concrete. Moreover, the piezoresistive capability of the element is used for modeling piezoresistivity of smart concrete. The geometry, node locations and the coordinate system for this type of element are shown in Figure 2.3. The element's faces are illustrated by the circled numbers. Distributed surface loads, such as pressures, may be applied to the element's surfaces.

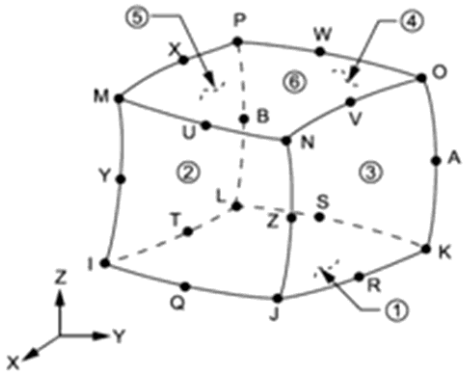

Figure 2.3 SOLID226 Element's geometry, node locations and coordinate system in ANSYS 14.0 (ANSYS)

2.2.3 Defining Material Properties

SOLID226 element requires elastic constants, electrical resistivity and piezoresistive matrix to properly model a piezoresistive material. These properties were taken from experimental investigation data of Teomete (2017) and used for the material model in the finite element model. The material properties used in the analyses are given in Table 2.2.

Elastic constants include the modulus of elasticity of the smart concrete (E), and the Poisson's ratio (υ). The elastic modulus of the smart concrete specimens was determined experimentally by using the slope of the tangent to the stress-strain curve. All of the specimens had the same Young's modulus (38 GPa) except Specimen 1, which had a higher Young's modulus (47 GPa). This may be due to the differences in handling during curing and testing. The Poisson's ratio was experimentally determined by strain measurements and was evaluated as 0.18.

The electrical resistivity of smart concrete prior to loading is necessary to simulate its piezoresistive behavior. Consequently, the initial electrical resistivity ρ_o of the tested specimens was considered as input in the finite element model of smart concrete. ρ_o was calculated by Equation 2.2. This equation means that the resistivity ρ is independent of the geometry and is thus a material property (Chung, 2010). On the contrary, the resistance R_s depends on the geometry such that it is proportional to L and inversely proportional to A.

For modeling of piezoresistive concrete, the piezoresistive matrix *[m]* is also required in finite element modeling. It is a non-symmetric 6 by 6 matrix that served to relate the X, Y and Z terms of compressive strain to the corresponding terms of electrical resistivity change via 3 constants m_x, m_y and m_z as shown in the following equation:

$$\begin{Bmatrix} \Delta\rho_x \\ \Delta\rho_y \\ \Delta\rho_z \\ \Delta\rho_{xy} \\ \Delta\rho_{yz} \\ \Delta\rho_{xz} \end{Bmatrix} = \begin{bmatrix} m_x & 0 & 0 & 0 & 0 & 0 \\ 0 & m_y & 0 & 0 & 0 & 0 \\ 0 & 0 & m_z & 0 & 0 & 0 \\ 0 & 0 & 0 & 0 & 0 & 0 \\ 0 & 0 & 0 & 0 & 0 & 0 \\ 0 & 0 & 0 & 0 & 0 & 0 \end{bmatrix} \times \begin{Bmatrix} \varepsilon_x \\ \varepsilon_y \\ \varepsilon_z \\ \gamma_{xy} \\ \gamma_{yz} \\ \gamma_{xz} \end{Bmatrix} \tag{2.4}$$

Equation 2.4 can be written in a compact form as

$$\{\Delta\rho\} = [m]\{\varepsilon\} \quad (2.5)$$

in which *{Δρ}* is the vector of change in electrical resistivity and *{ε}* is the elastic strain vector with normal strain components (ε_x, ε_y, ε_z) and shear strain components (γ_{xy}, γ_{yz}, γ_{xz}).

In *[m]* matrix, the m_x, m_y and m_z piezoresistive coefficients express the relative change in resistivity due to normal strain. The *X*, *Y* and *Z* subscripts refer to the change in resistivity in one direction (*X*, *Y* or *Z* direction) caused by the applied strain in the same direction (*X*, *Y* or *Z* direction). In this study, the numerical model of smart concrete was assumed to be an isotropic material. Therefore, only m_x, m_y and m_z coefficients were considered. Any additional coefficient was ignored. These coefficients were taken from the strain sensitivity data of the smart concrete specimens obtained from compression test, which was evaluated as the change in electrical resistivity per unit strain.

Table 2.2 The material properties of smart concrete numerical models

FE Model	**Young's Modulus, *E* (Pa)**	**Poisson's Ratio, *υ***	**Electrical Resistivity, ρ_O (Ωm)**	**Piezoresistive Coefficients, m_x, m_y, m_z**
FE-1	47×10^9	0.18	358.665	66.85
FE-2	38×10^9	0.18	356.433	51.79
FE-3	38×10^9	0.18	374.368	44.82

2.2.4 Creating The Model Geometry

The geometrical representation of the physical system is referred to as the solid model (Madenci & Güven, 2006). The created solid model must be discretized in terms of nodes and elements in order to generate a finite element mesh and ultimately apply finite element analysis. There are two main ways offered in modeling the geometry part: (1) solid modeling and meshing and (2) direct generation. Solid modeling allows the user to create the geometric boundaries of the

model, such as lines, areas or volumes and to control the size and shape of finite elements, then the meshing process is accomplished by using an automated finite element mesh operator. By contrast, in direct generation method, the coordinates of every single node and the size, shape, and connectivity of every single element are determined prior to defining these entities in the finite element model. Direct generation is more convenient for small or simple models than is solid modeling. However, for ease of modeling of three-dimensional models, solid modeling method was prefered in this study.

The smart concrete cube specimens were modeled as volumes. The dimensions were input in meter (*m*). All the models were 0.075m long with a cross-section of 0.075 × 0.075 m. During creation of the geometry, each solid model was first formulated as 5 distinct rectangular blocks; the lines separating the blocks served as location of electrodes. An individual block was 0.075m long. The middle block lying between the inner two electrodes E_v had a height of 0.035 m; its height symbolizes the gage length of the specimen. The 4 remaining blocks had a height of 0.010 m; their height illustrates the distance between inner and outer electrodes. All the 5 blocks were later combined using the glue operation. Glue operation is a Boolean operation utilized for connecting solid model entities that are touching one another but not sharing any part. At the end of the operation, no additional block was created but new parts that have one lower dimensionality (i.e. areas of intersection between adjacent blocks) were produced. Figure 2.4 depicts a typical whole size solid model of smart concrete with intersecting lines representing the position of inner and outer electrodes.

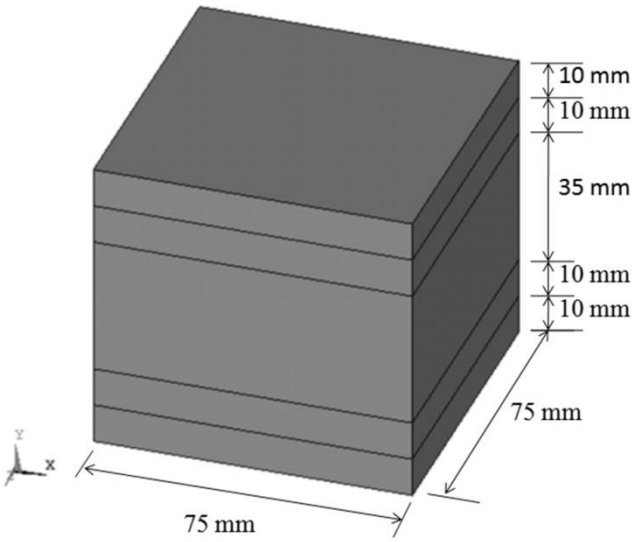

Figure 2.4 The smart concrete solid model (ANSYS)

2.2.5 Generating The Mesh

After establishing material properties and building the solid model, meshing was performed. The element edge size can be set for better solution accuracy, i.e. a mesh with all elements having edge sizes as close as possible to the specified value can be generated. Additionally, a resonable number of elements can be selected to get accurate results and minimize analysis time.

In this study, 20-node hexahedral (brick) coupled-field solid elements SOLID226 which are described in section 2.2.2 were used. They had 0.0075 m size each. Figure 2.5 shows the result of the meshing operation of the solid model: 10 elements along lines on the length and width of the model were produced. Moreover, 13 elements were created by the height of the model, i.e. 5 elements along the height (0.035 m) of the middle volume and 8 elements along the heights (0.010 m) of the remaining 4 volumes. Mesh refinement was performed until the changes in the results are significantly small. The overall mesh comprises 1300 elements and 6347 nodes.

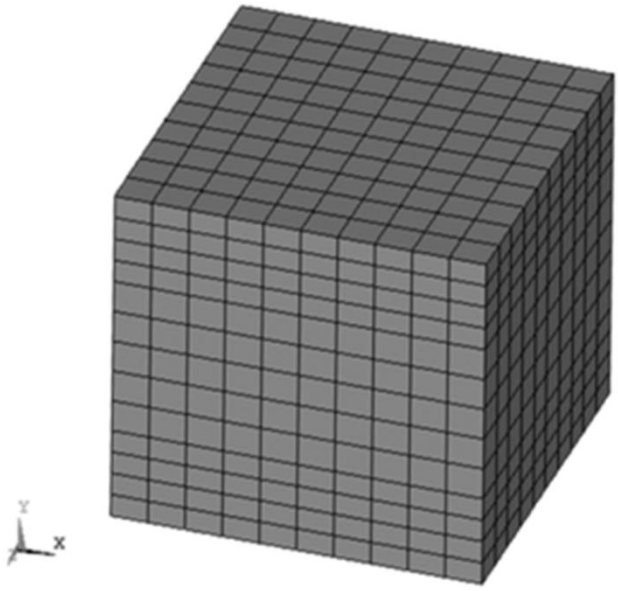

Figure 2.5 The finite element mesh of smart concrete model (ANSYS)

2.2.6 Loading Conditions

The word loads in ANSYS terminology includes boundary conditions and externally or internally applied forces. The present problem requires application of displacement and voltage boundary conditions to the finite element (FE) model in order to simulate the actual structural support system and the current supply through electrodes. The pressure applied on the specimens can also be modeled in the form of surface or distributed loads applied either on the solid model (areas) or on the finite element model (nodes located on areas).

In this study, the FE model was restrained vertically (in Y direction) at the bottom and was free in the horizontal (X and Z) directions, as it was tested experimentally. Figure 2.6 shows the vertical constraints at the bottom of the numerical model, with *UY* (displacement translation in Y direction) equal to zero.

The electrodes of the model were simulated by coupling *VOLT* (voltage) degree of freedom of the nodes located on the electrodes. Coupling (CP) is essential if a particular DOF is expected to have the same value at several nodes (Madenci & Güven, 2006). In this study, 20V DC current was decreased by the potential

difference across the reference resistance V_r for every pressure. The obtained current was supplied through the nodes located at the position of the outer electrodes. The nodes occupying the place of inner electrodes were also coupled in *VOLT* DOF in order to further read the output potential difference across the FE model. In Figure 2.6, the black dots represent the nodes of a finite element model viewed in XY plane. The electrodes are shown by coupled set of nodes in green.

The pressure applied on the specimens was modeled as nodal pressure, i.e a pressure loading acting on nodes located at the top area of the finite element model. The ANSYS convention for pressure loading is that a positive load value represents pressure into the surface (compressive). Figure 2.6 illustrates pressure load applied on top nodes (red arrows).

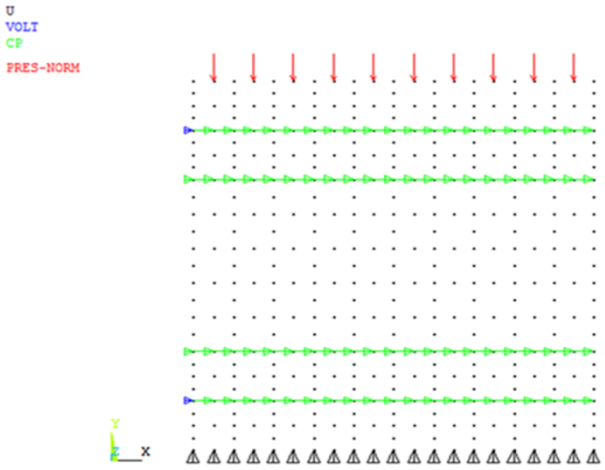

Figure 2.6 The loading conditions of a finite element model in XY Plane, with vertical displacement constraint (U), coupled (CP) voltage constraint (VOLT) at electrodes, and distributed load pressure (PRES-NORM) (ANSYS)

2.2.7 Solution in Single Step, Load Steps and Piecewise Steps

After completing the finite element mesh and specifying the loading conditions (boundary and surface loads), the finite element solution was achieved by considering three different cases: (1) single step, (2) multiple load steps and (3) piecewise steps. A step corresponds to a set of loads for which the analyst wants to

obtain a solution and review the results. Table 2.3 presents the details of the analyses conducted in the present work.

In single step method, a single pressure load was applied individually to the appropriate nodes in a single static analysis. 8 static pressures were selected based on compression test: 0.018, 5, 10, 20, 30, 40, 50 and 51.58 MPa. The first selected pressure was taken as the unloaded state of the specimens. The last selected pressure equals to the ultimate load of the tested smart concrete specimens. These pressures were applied at the nodes located on top area of the model, at location Y=0.075m. A total of 8 piezoresistive static analyses were separately conducted. The unit of pressure adopted throughout the modeling was Pascal (Pa).

In load steps method, time-dependent pressure loads were applied through the use of load steps in the same static analysis. A load step is a configuration of loads for which a solution is obtained. In this study, the loads and specimen's response were assumed to vary slowly with respect to time. In this case, the first load step corresponding to 0.018 MPa pressure load ended at time = 1, then the second load step corresponding to 5 MPa proceeded until time=2, and so on. A total of 8 load steps were gradually achieved within a single static analysis with the last load step equal to 51.58 MPa.

In piecewise steps method, 4 different static analyses were conducted separately. In these analyses, the last load steps were equal to 5, 20, 40 and 51.58 MPa, respectively. The last load step of the first static analysis (5 MPa) corresponded to the first load step of the subsequent analysis .

Table 2.3 The details of numerical methods used in finite element analyses

Numerical Method	Pressure Loads (MPa)
Single Step	0.018 – 5 – 10 – 20 – 30 – 40 – 50 – 51.58
Load Steps	0.018 5 10 20 30 40 50 51.58
Piecewise Steps	0.018 2 5
	5 10 20
	20 30 40
	40 50 51.8

2.2.8 Evaluation of The Numerical Results

The electrical resistivity change in the finite element model is caused by the applied strain. In order to compute the electrical resistivity of models, two different ways can be followed.

In the first way, the electric field and the current density (defined as the current I per unit cross-sectional area A) at different loads were determined from the analysis by element solution. In this case, the electrical resistivity ρ_m of the finite element models at different applied loads was computed using

$$\rho_m = \frac{E}{J} \tag{2.6}$$

in which E denotes the output electric field vector sum (V/m) by element solution and J is the output current density vector sum (A/m^2) by element solution (Chung, 2010; Mason & Thurston, 1957; Mohammed, Moussa & Lou, 2008).

In the second way, the electrical resistance of the models at each point of the analysis was computed using the output current I by element solution and the output potential difference V read from the coupled inner voltage electrodes E_v of the models by applying Ohm's law:

$$R = \frac{V}{I} \tag{2.7}$$

In this case, the electrical resistivity ρ_e of the finite element models at each point of the analysis was evaluated by

$$\rho_e = \frac{A}{L} \times R \tag{2.8}$$

where R is the output electrical resistance (Ω) by element solution, L the length between inner voltage electrodes (m) and A is the cross-section area of the model (m^2).

In all the cases, the electrical resistivity change of finite element models was computed in virtue of Equation 2.3. The output strain at each pressure load was also

retrieved from the analysis. The finite element results were compared with experimental results.

CHAPTER THREE
RESULTS AND DISCUSSION

The numerical results and discussion are presented in this chapter. The results obtained from single step, load steps and piecewise steps methods were compared to experimental results gathered from the work of Teomete (2017).

The numerical contour plots of stress, strain, electric field and current density by element solution were given for the maximum and minimum pressure loads in single step method. The same contour plots were sketched for the first and last load steps and compared in load steps and piecewise steps methods. The output voltage and output current were obtained from the model. The electrical resistivity was evaluated from both Equations 2.6 and 2.8 and the results were compared in single step method. The electrical resistivity change % ρ – strain graph was plotted with experimental result obtained from compression test.

The experimental results of 3 compression tests conducted on 3 smart concrete samples (Specimen 1, 2 and 3) were modeled as FE-1, FE-2 and FE-3.

3.1 Numerical Results Using Single Step Method

8 different pressure loads were separately applied on the three finite element models FE-1, FE-2 and FE-3. Each load corresponded to a single static analysis. By default, the program automatically assigned time = 1 at the end of each load as a counter in single step method. 0.018 MPa was chosen as the unloaded state of the specimens. 51.58 MPa was the ultimate load of the samples. In this method, the results gathered from the minimum pressure load (0.018 MPa) were compared with the results obtained from the maximum pressure load (51.58 MPa). Table 3.1 presents a summary of the decrease of electrical resistivity (%) obtained in experiments, as well as in numerical models using single step method.

Table 3.1 The decrease of electrical resistivity (%) obtained from experimental results and FE models using single step method

	FE Model	FE Model Using Equation 2.6 (E/J Model)	FE Model Using Equation 2.8 (V/I Model)	Experimental Results
Electrical Resistivity Decrease (%)	FE-1	7.3	7	6.8
	FE-2	7	6.9	7
	FE-3	6	6	6.8

3.1.1 Numerical Results of Finite Element Model FE-1

The numerical contour plots of stress and strain by element solution obtained for the minimum (0.018 MPa) and maximum (51.58 MPa) pressure loads are given in Figures 3.1 and 3.2, respectively. As can be seen in Figures 3.1 (a) and (b), the stress in Y direction (output as SY) is a single value and is equal to the applied pressure load (-18000 Pa and -51600000 Pa, for the minimum and maximum pressure load, respectively). Similarly, the elastic strain in Y direction (output as EPELY) is a single value and equals to -0.383×10^{-6} for the minimum and -0.001097 for the maximum load, as illustrated in Figures 3.2 (a) and (b). The ultimate compressive strain obtained from experiment (-0.001057) and the maximum compressive strain obtained from simulation (-0.001097) are close to each other.

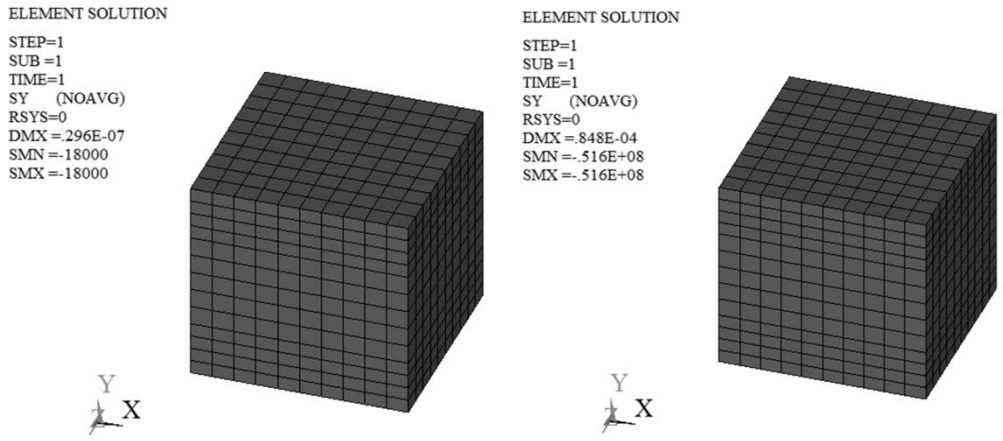

(a) (b)

Figure 3.1 The stress contour plots in Y direction (SY) by element solution for (a) the minimum (0.018 MPa) and (b) maximum (51.58 MPa) pressure loads of FE-1 model

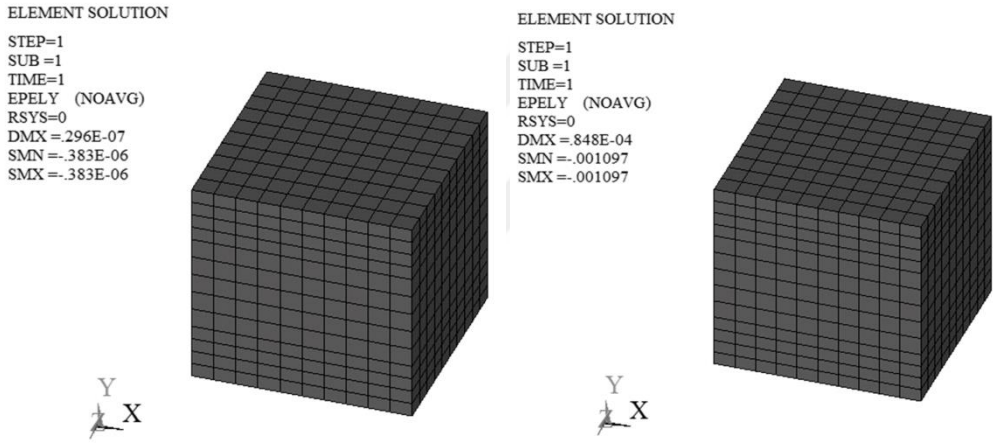

(a) (b)

Figure 3.2 The strain contour plots in Y direction (EPELY) by element solution for (a) the minimum (0.018 MPa) and (b) the maximum (51.58 MPa) pressure loads of FE-1 model

The numerical contour plots of electric field and current density vector sum by element solution for the minimum (0.018 MPa) and maximum (51.58 MPa) pressure loads are compared in Figures 3.3 and 3.4, respectively. The electric field (output as EFSUM) decreased from 280 V/m (obtained at the lowest pressure level) to 276.364 V/m (at the highest pressure level), while the current density (output as JSSUM) increased from 0.780693 A/m^2 to 0.831539 A/m^2.

As explained in the second chapter, one way to calculate the electrical resistivity of finite element models was by dividing the electric field vector sum to the current density vector sum as shown in Equation 2.6. By using this equation, the electrical resistivity in FE-1 model for the minimum (0.018 MPa) and maximum (51.58 MPa) pressure loads was computed as 358.67 Ωm and 332.35 Ωm, respectively. The electrical resistivity in Specimen 1 at the minimum and maximum stress was respectively measured as 358.65 Ωm and 334.17 Ωm. In this case, the resistivity decreased by 7.3% and 6.8% in the numerical model and experimental results, respectively, from the minimum to the maximum pressure load.

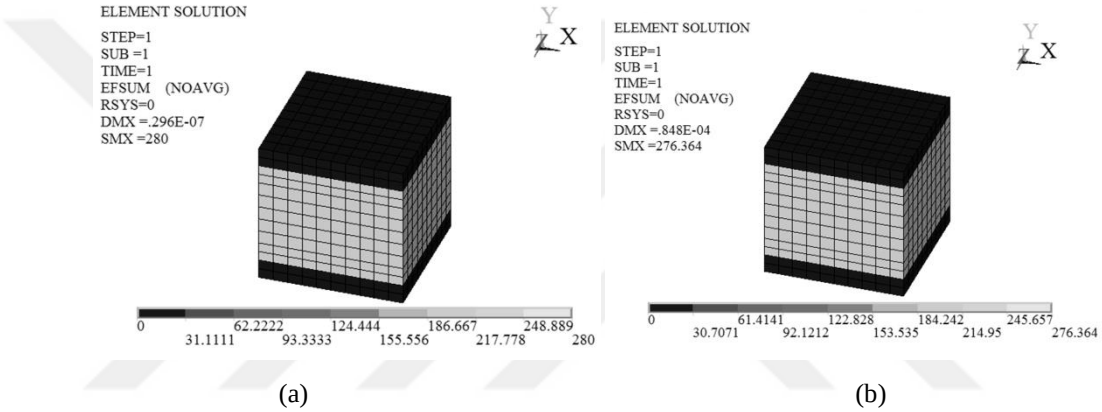

(a) (b)

Figure 3.3 The numerical contour plots of electric field vector sum (EFSUM) by element solution for (a) the minimum (0.018 MPa) and (b) the maximum (51.58 MPa) pressure loads of FE-1 model

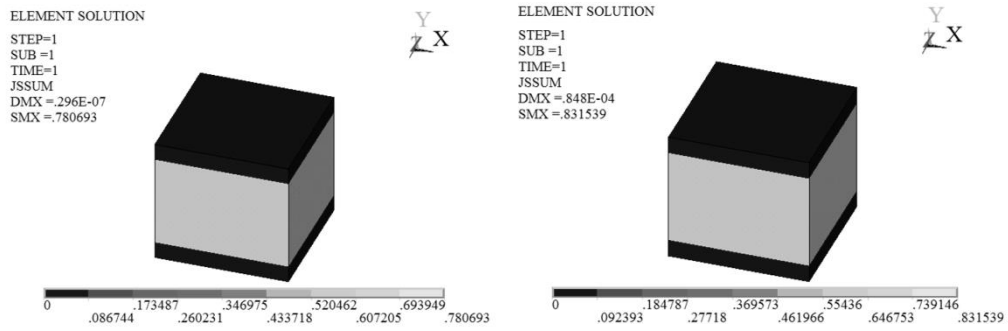

(a) (b)

Figure 3.4 The numerical contour plots of current density vector sum (JSSUM) by element solution for (a) the minimum (0.018 MPa) and (b) the maximum (51.58 MPa) pressure loads of FE-1 model

The electrical resistivity of finite element models was calculated in the second way by use of Ohm's law and Equation 2.8. The electrical resistivity in FE-1 model

for the minimum (0.018 MPa) and maximum (51.58 MPa) pressure loads were computed as 358.65 Ωm and 333.28 Ωm, respectively. The electrical resistivity in Specimen 1 for the minimum and maximum pressure loads was respectively equal to 358.67 Ωm and 334.17 Ωm, as discussed earlier. In this case, the resistivity decreased by 7% and 6.8% in the numerical model and experimental results, respectively.

The output voltage was obtained from coupled voltage electrodes E_v of FE-1 model, while the output current of the model was retrieved as reaction solution from the piezoresistive analysis. The output voltage at the minimum and maximum pressure was individually equal to 9.8 V and 9.7 V. The output current passing through FE-1 model at the minimum and maximum pressure was respectively equal to 0.0043914 A and 0.0046774 A. These simulation values were compared with experimental results. It was observed that the minimum and the maximum electrical potential difference across Specimen 1 was measured as 10.2 V and 10 V, respectively. The electric current was respectively equal to 0.004583 A and 0.004795 A, at the minimum and maximum stress level. In Specimen 1 and FE-1 model, the potential difference decreased from the lowest to the highest pressure level, while the electric current increased.

The experimental results of Teomete (2017) are plotted with the numerical results obtained from FE-1 model in Figure 3.5. The evaluation of electrical resistivity by use of Equation 2.6 and Equation 2.8 (E/J model and V/I model, respectively) indicate that all the curves followed similar trend. The electrical resistivity in numerical model decreased with the applied strain, which is also observed in experimental results. The % ρ took negative values, which means the electrical resistivity of the specimen decreased during the test and the analysis. This decrease can be explained by the effect of the vertical compressive strain on microvoid closure and the subsequent increase of the fiber-matrix and fiber-fiber contact (Teomete, 2017).

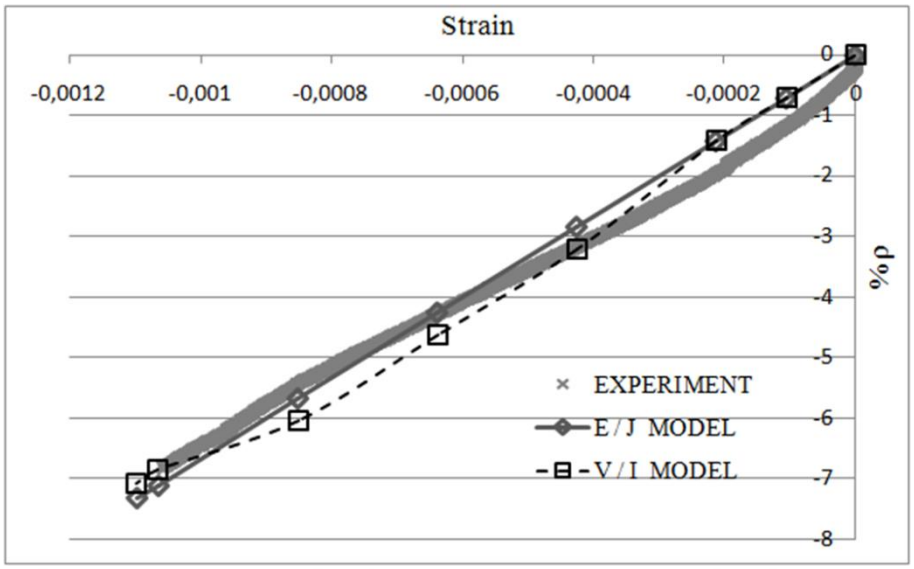

Figure 3.5 Experimental and FEM % ρ – strain graphs using single step method; smart concrete specimen 1 vs FE-1 model

3.1.2 Numerical Results of Finite Element Model FE-2

Figures 3.6 and 3.7 illustrate the contour plots of stress and strain by element solution for the minimum (0.018 MPa) and maximum (51.58 MPa) pressure loads, respectively. The stress in Y direction (SY) is a single value and is equal to the applied pressure load (-18000 Pa and -51600000 Pa), as can be seen in Figures 3.6 (a) and (b). The elastic strain in Y direction (EPELY) is a single value and equals to -0.474×10^{-6} and -0.001357 for the minimum and maximum load, see Figures 3.7 (a) and (b). The ultimate compressive strain obtained from experiment (-0.001351) and the maximum compressive strain from FE-2 model (-0.001357) are almost equal.

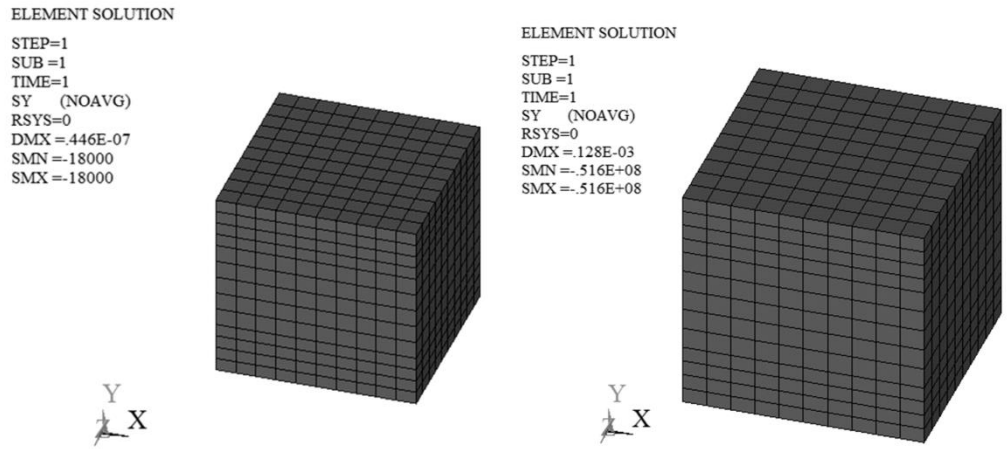

(a) (b)

Figure 3.6 The stress contour plots in Y direction (SY) by element solution for (a) the minimum (0.018 MPa) and (b) the maximum (51.58 MPa) pressure loads of FE-2 model

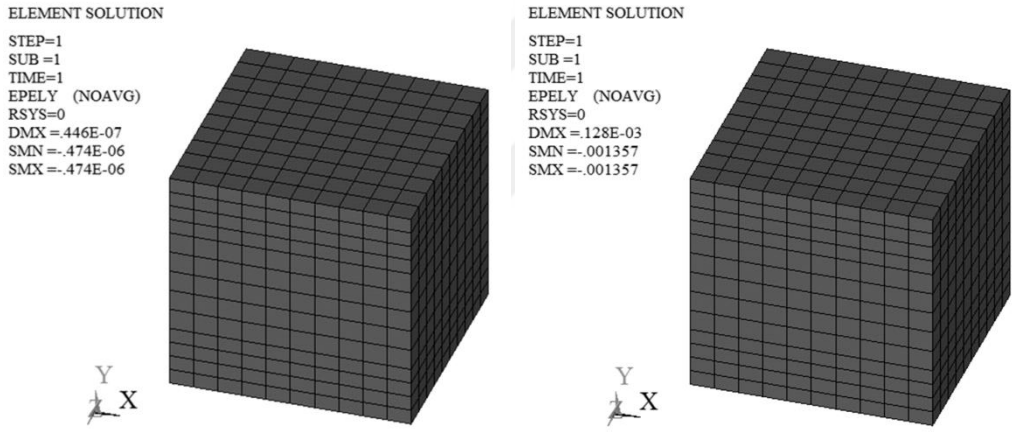

(a) (b)

Figure 3.7 The strain contour plots in Y direction (EPELY) by element solution for (a) the minimum (0.018 MPa) and (b) the maximum (51.58 MPa) pressure loads of FE-2 model

Figures 3.8 and 3.9 show a comparison of the numerical contour plots of electric field (EFSUM) and current density (JSSUM) vector sum by element solution for the minimum and maximum pressure loads, respectively. As the electric field decreased from the lowest to the highest stress level (from 283.636 V/m to 278.182 V/m), the current density increased from 0.795783 A/m^2 to 0.839474 A/m^2.

By using Equation 2.6, the electrical resistivity in FE-2 model for the minimum and maximum pressure loads was calculated as 356.42 Ωm and 331.38 Ωm,

respectively. The electrical resistivity in Specimen 2 for the minimum and maximum pressure loads was respectively equal to 356.43 Ωm and 331.43 Ωm. In this case, the resistivity decreased by 7% in both the numerical model and experimental results, from minimum to maximum load.

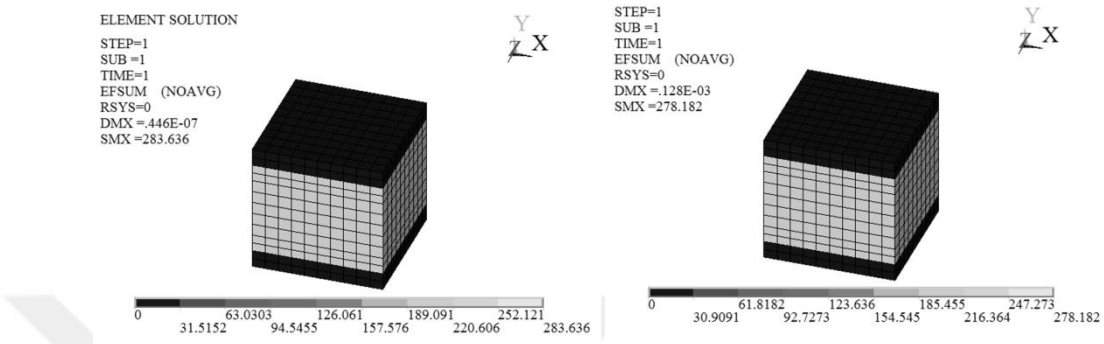

(a) (b)

Figure 3.8 The numerical contour plots of electric field vector sum (EFSUM) by element solution for (a) the minimum (0.018 MPa) and (b) the maximum (51.58 MPa) pressure loads of FE-2 model

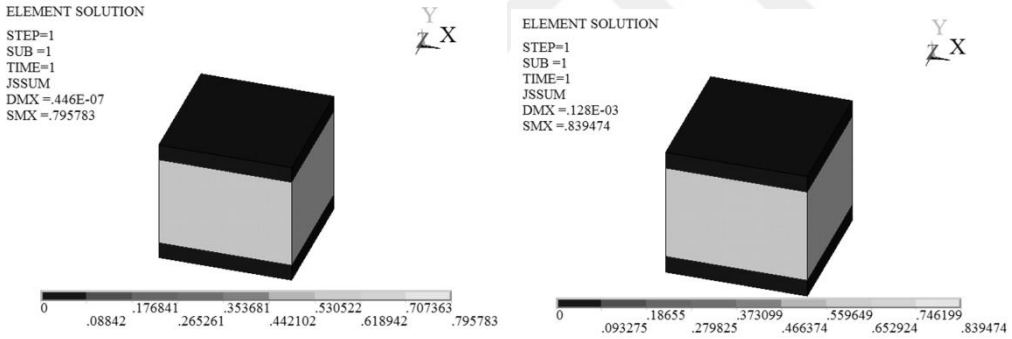

(a) (b)

Figure 3.9 The numerical contour plots of current density vector sum (JSSUM) by element solution for (a) the minimum (0.018 MPa) and (b) the maximum (51.58 MPa) pressure loads of FE-2 model

The use of Ohm's law and Equation 2.8 allowed to calculate the electrical resistivity in FE-2 model for the minimum and maximum pressure loads. It was calculated as 356.16 Ωm and 331.5 Ωm, respectively. As mentioned above, the electrical resistivity in Specimen 2 for the minimum and maximum pressure loads was respectively equal to 356.43 Ωm and 331.43 Ωm. In this case, the resistivity decrease obtained from the model and experimental results is 6.9% and 7%, respectively, considering the minimum and maximum pressure loads.

The output voltage at the minimum and maximum pressure was determined from the inner voltage electrodes of FE-2 model as 9.9 V and 9.7 V. The output current passing through FE-2 model at the minimum and maximum pressure was respectively equal to 0.0044763 A and 0.004722 A. In the same manner, the potential difference measured across Specimen 2 was equal to 9.8 V and 9.6 V, respectively, while the electric current was respectively equal to 0.004429 A and 0.004651 A, at the minimum and maximum stress level. In both Specimen 2 and FE-2 model, the potential difference decreased from the minimum to the maximum pressure load, while the electric current increased.

Figure 3.10 shows the resistivity change % ρ – strain graph for Specimen 2 from the experiments plotted with the finite element results. For both Equations 2.6 and 2.8 (E/J Model and V/I Model), simulation values match with experimental results. The decrease of electrical resistivity was due to compressive strain which led to closure of microcracks and microvoids and increased the fiber-matrix and fiber-fiber contact (Teomete, 2017).

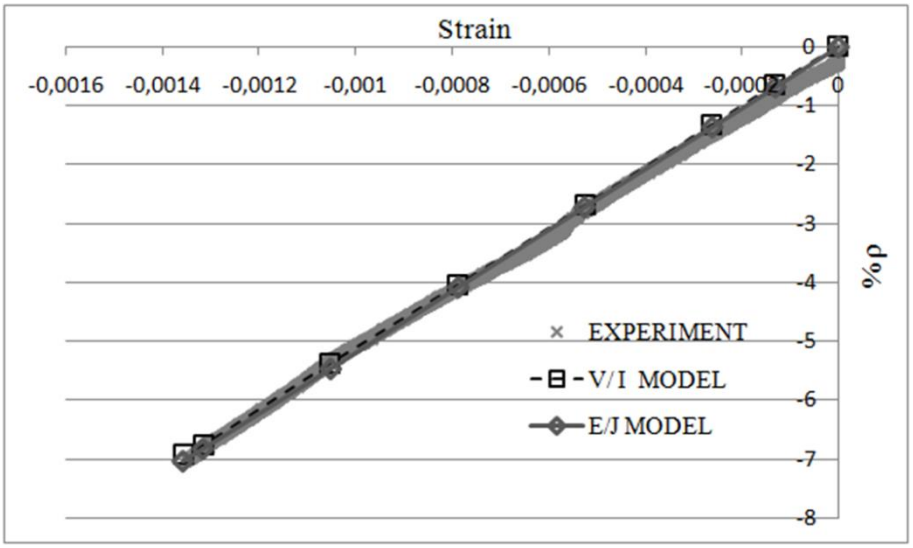

Figure 3.10 Experimental and FEM % ρ – strain graphs using single step method; smart concrete specimen 2 vs FE-2 model

3.1.3 Numerical Results of Finite Element Model FE-3

Contour plots of strain and stress by element solution for the minimum (0.018 MPa) and maximum (51.58 MPa) pressure loads are shown in Figures 3.11 and 3.12, respectively. Since the analysis is of static type, the obtained output strain in Y direction (EPELY) matched with the applied compressive strain: -0.474×10^{-6} for the lowest and -0.001357 for the highest load. Similarly, the output stress in Y direction (SY) obtained at the minimum and maximum load corresponded to the applied pressure: -18000 Pa and -51600000 Pa, respectively. The ultimate compressive strain obtained from Specimen 3 (-0.001476) is close to the maximum compressive strain computed in FE-3 model (-0.001357).

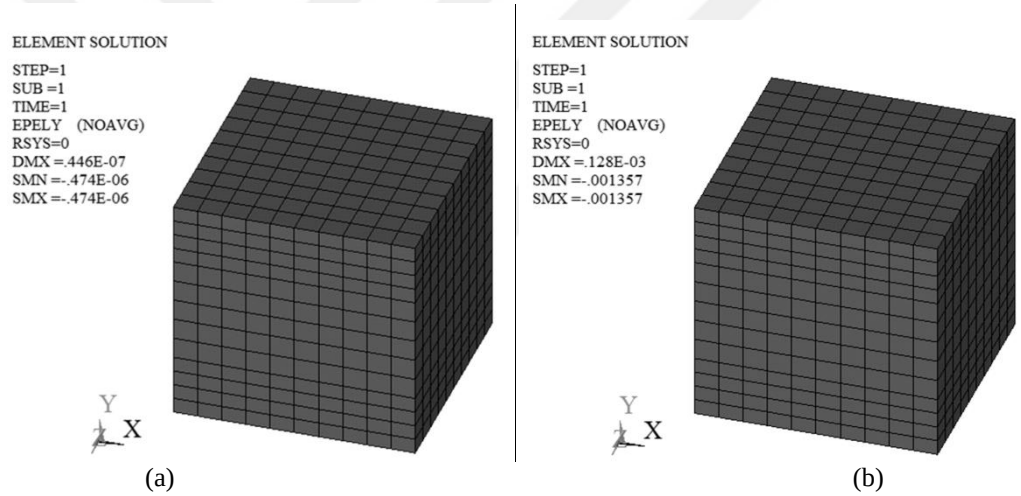

(a) (b)

Figure 3.11 The strain contour plots in Y direction (EPELY) by element solution for (a) the minimum (0.018 MPa) and (b) the maximum (51.58 MPa) pressure loads of FE-3 model

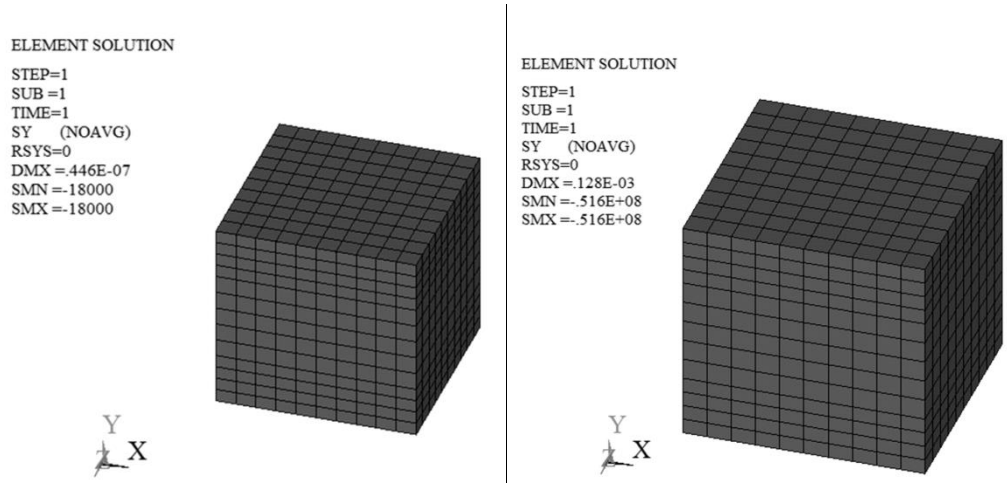

(a) (b)

Figure 3.12 The stress contour plots in Y direction (SY) by element solution for (a) the minimum (0.018 MPa) and (b) the maximum (51.58 MPa) pressure loads of FE-3 model

Contour plots of current density and electric field vector sum by element solution for the minimum and maximum pressure loads are given in Figures 3.13 and 3.14, respectively. There was an increase of the current density from the lowest to the highest pressure level, while a decrease of the electric field was noticed.

The electrical resistivity in Specimen 3 for the minimum and maximum pressure loads was respectively equal to 374.37 Ωm and 348.93 Ωm. The electrical resistivity in FE-3 model for the minimum and maximum pressure loads was computed as 374.36 Ωm and 351.59 Ωm, respectively, by use of Equation 2.6. The resistivity was lessened by 6.8% and 6% in the experimental results and numerical model, respectively, for the minimum and maximum load.

The electrical resistivity in FE-3 model was also derived using Ohm's law. It was respectively equal to 374.08 Ωm and 351.59 Ωm, for the minimum and maximum pressure loads. In this case, the resistivity was also decreased by 6% in FE-3 model for the minimum and maximum pressure loads.

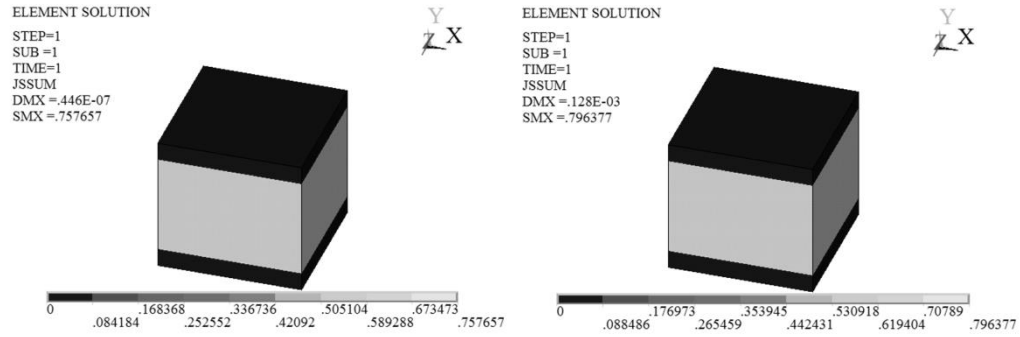

(a) (b)

Figure 3.13 The numerical contour plots of current density vector sum (JSSUM) by element solution for (a) the minimum (0.018 MPa) and (b) the maximum (51.58 MPa) pressure loads of FE-3 model

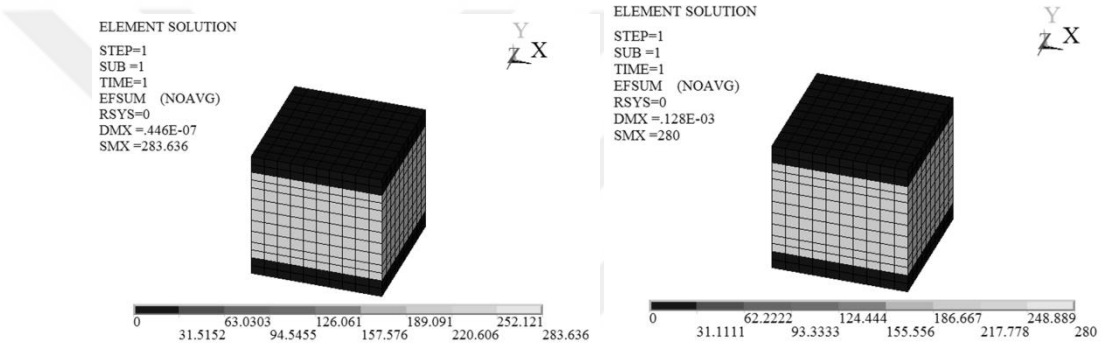

(a) (b)

Figure 3.14 The numerical contour plots of electric field vector sum (EFSUM) by element solution for (a) the minimum (0.018 MPa) and (b) the maximum (51.58 MPa) pressure loads of FE-3 model

At the minimum and maximum stress, the electrical potential difference across Specimen 3 was measured as 10.1 V and 10 V, respectively. Simultaneously, the electric current was found to be equal to 0.004347 A and 0.004595 A. The voltage read from the electrodes of FE-3 model was listed as 9.9 V and 9.8 V, for the minimum and maximum pressure. The output current passing through the model at the minimum and maximum pressure was obtained as 0.0042618 A and 0.0044796 A. The potential difference decreased from the lowest to the highest stress level, while the electric current increased, in both Specimen 3 and FE-3 model.

Figure 3.15 shows good correlation between the resistivity change % ρ and the elastic strain for both experimental and model results. Note that evaluations using Equations 2.6 and 2.8 (E/J Model and V/I Model) provide the same results: the

electrical resistivity in FE-3 model decreases with the applied strain, which is also observed in experimental results. The strong linear relationship between electrical resistivity and strain implies that there is good strain sensitivity within the tested smart concrete specimens (Teomete, 2017).

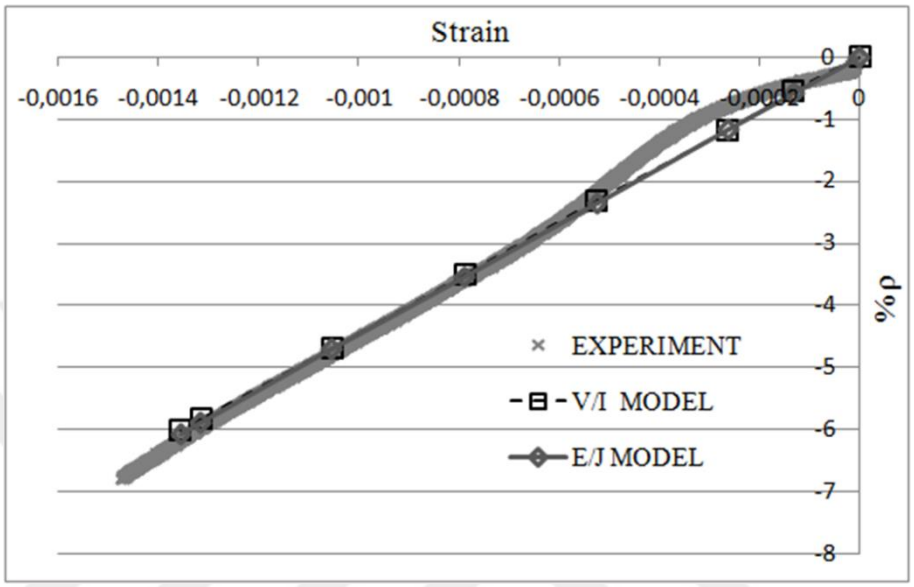

Figure 3.15 Experimental and FEM % ρ – strain graphs using single step method; smart concrete specimen 3 vs FE-3 model

3.2 Numerical Results Using Load Steps Method

8 load steps were defined and solved sequentially in a single piezoresistive static analysis. The first load step corresponded to 0.018MPa (specimens' unloaded state), while the last load step corresponded to 51.58 MPa. The analysis was conducted on the three finite element models FE-1, FE-2 and FE-3. Time was assigned at the end of each load step, so that the applied loads may vary incrementally over the 8 load steps. In this method, the results gathered from the first load step (0.018 MPa) were compared with the results obtained from the last load step (51.58 MPa). The resistivity of finite element models was calculated using Equation 2.6. A summary of the decrease of electrical resistivity (%) obtained in specimens, as well as in numerical models using load steps method is tabulated in Table 3.2.

Table 3.2 The decrease of electrical resistivity (%) obtained in specimens and FE models using load steps method

Electrical Resistivity Decrease (%)	FE Model	FE Model Using Equation 2.6 (E/J Model)	Experimental results
	FE-1	7.1	6.8
	FE-2	7	7
	FE-3	6	6.8

3.2.1 Numerical Results of Finite Element Model FE-1

Stress and strain contour plots by element solution for the first (0.018 MPa) and last (51.58 MPa) load steps are given in Figures 3.16 and 3.17, respectively. Figures 3.16 (a) and (b) point out the stress in Y direction, output as SY, as a single value; it is equal to the applied minimum and maximum pressure load (-18000 Pa and -51600000 Pa), respectively. Figures 3.17 (a) and (b) refer to the elastic strain in Y direction, output as EPELY, as a single value; it corresponds to the calculated compressive strain (-0.383×10^{-6} and -0.001097). The ultimate compressive strain obtained from experiment (-0.001057) and the maximum compressive strain in FE-1 model (-0.001097) are approximately equal.

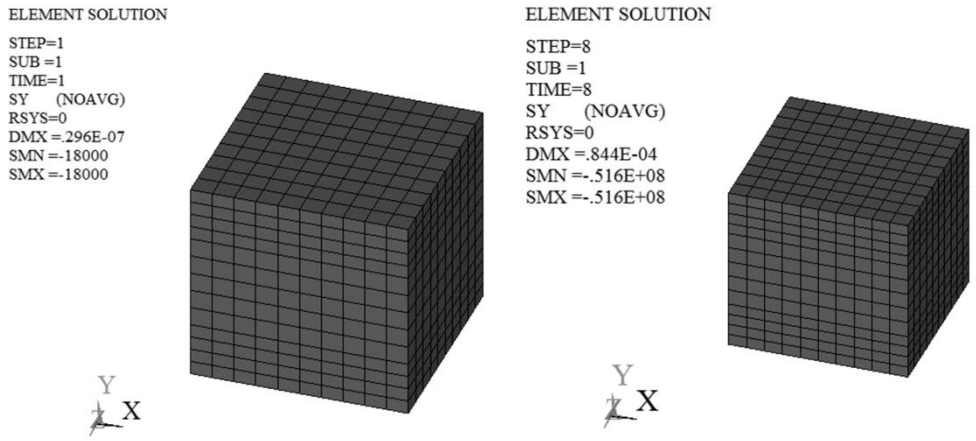

(a) (b)

Figure 3.16 The stress contour plots in Y direction (SY) by element solution for (a) the first (0.018 MPa) and (b) the last (51.58 MPa) load steps of FE-1 model

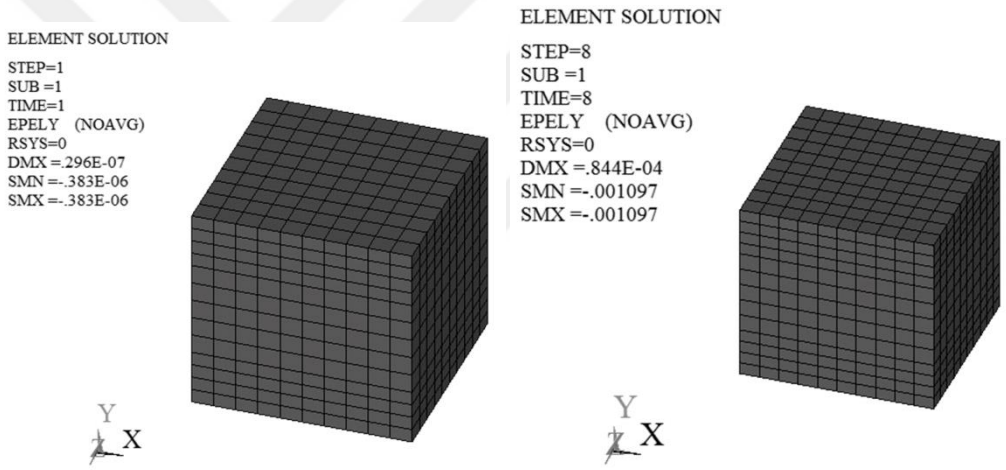

(a) (b)

Figure 3.17 The strain contour plots in Y direction (EPELY) by element solution for (a) the first (0.018 MPa) and (b) the last (51.58 MPa) load steps of FE-1 model

Electric field and current density vector sum contour plots by element solution for the first and last load steps are compared in Figures 3.18 and 3.19, respectively. It can be seen that the electric field decreased from the lowest to the highest pressure level, while the current density increased. The electrical resistivity of finite element models was then evaluated by dividing the electric field vector sum to the current density vector sum. The electrical resistivity in FE-1 model for the first and last load steps was obtained as 358.66 Ωm and 333.23 Ωm, respectively. The electrical resistivity in Specimen 1 for the minimum and maximum stress was respectively

equal to 358.65 Ωm and 334.17 Ωm. The resistivity decreased by 7.1% and 6.8% in the model and experiment, respectively. The electrical resistivities obtained from the model were very close to experimental results.

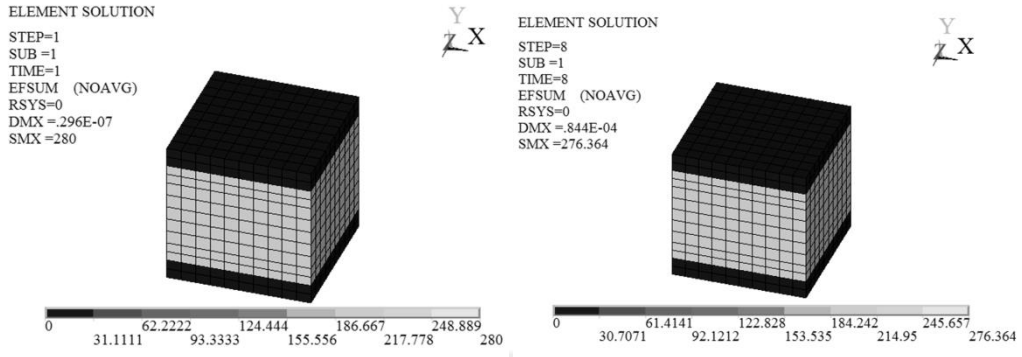

(a) (b)

Figure 3.18 The numerical contour plots of electric field vector sum (EFSUM) by element solution for (a) the first (0.018 MPa) and (b) the last (51.58 MPa) load steps of FE-1 model

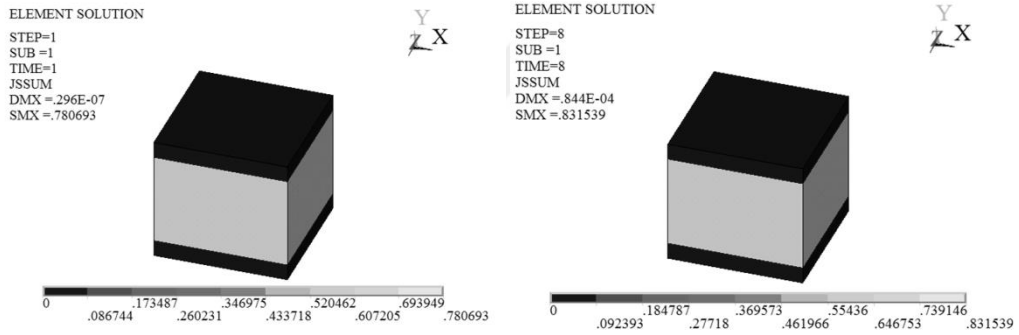

(a) (b)

Figure 3.19 The numerical contour plots of current density vector sum (JSSUM) by element solution for (a) the first (0.018 MPa) and (b) the last (51.58 MPa) load steps of FE-1 model

The results of FE analysis of Specimen 1 with the resistivity change % ρ - strain graph gathered from the experimental measurements are shown in Figure 3.20. As has been observed in experimental results, the electrical resistivity in numerical model also decreases with the applied strain.

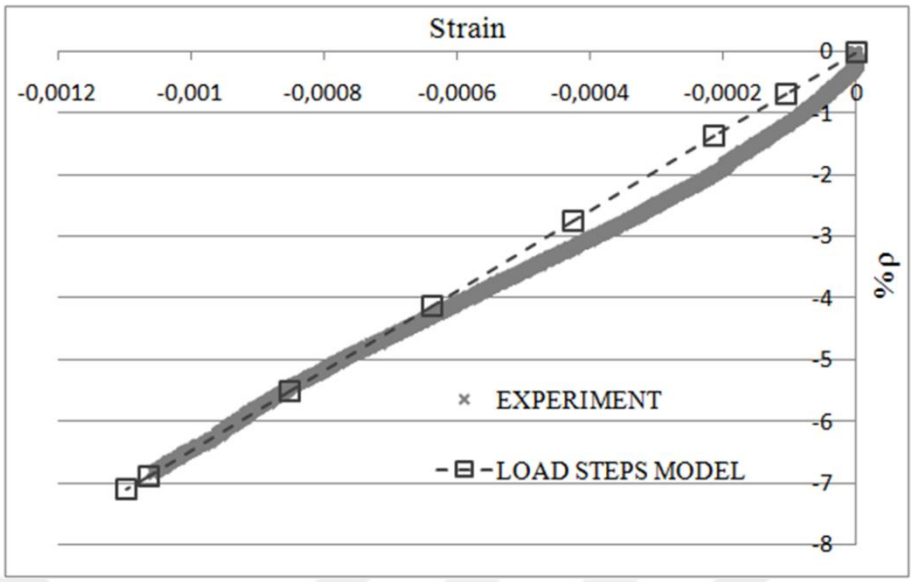

Figure 3.20 Experimental and FEM % ρ – strain graphs using load steps method; smart concrete specimen 1 vs FE-1 model

3.2.2 Numerical Results of Finite Element Model FE-2

In Figures 3.21 and 3.22, the solution output of stress and strain by element solution for the first and last load steps of FE-2 model are emphasized. The stress in vertical direction and the corresponding elastic strain are single values: -18000 Pa and -51600000 Pa for stress, and -0.474×10^{-6} and -0.001357 for strain, respectively, as obtained in the first and last load steps. The ultimate compressive strain measured from experiments (-0.001351) and the maximum compressive strain from FE-2 model (-0.001357) are practically equal.

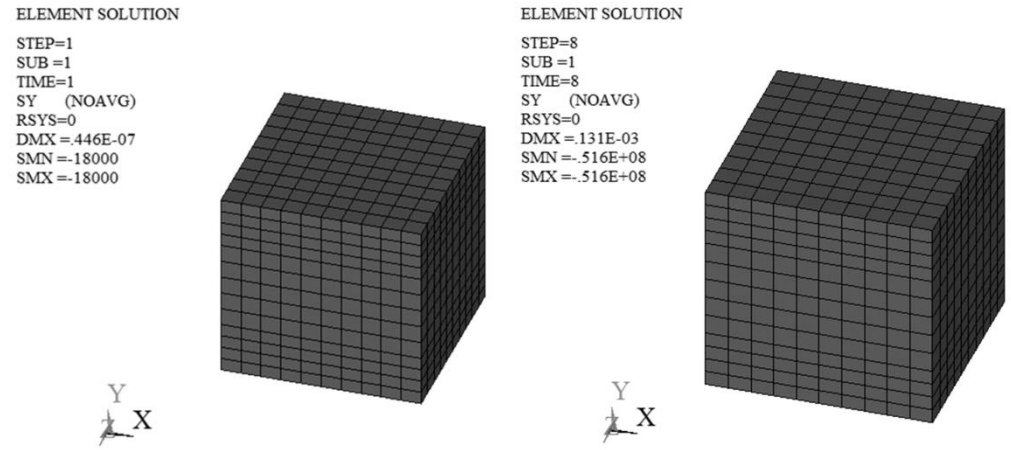

(a) (b)

Figure 3.21 The stress contour plots in Y direction (SY) by element solution for (a) the first (0.018 MPa) and (b) the last (51.58 MPa) load steps of FE-2 model

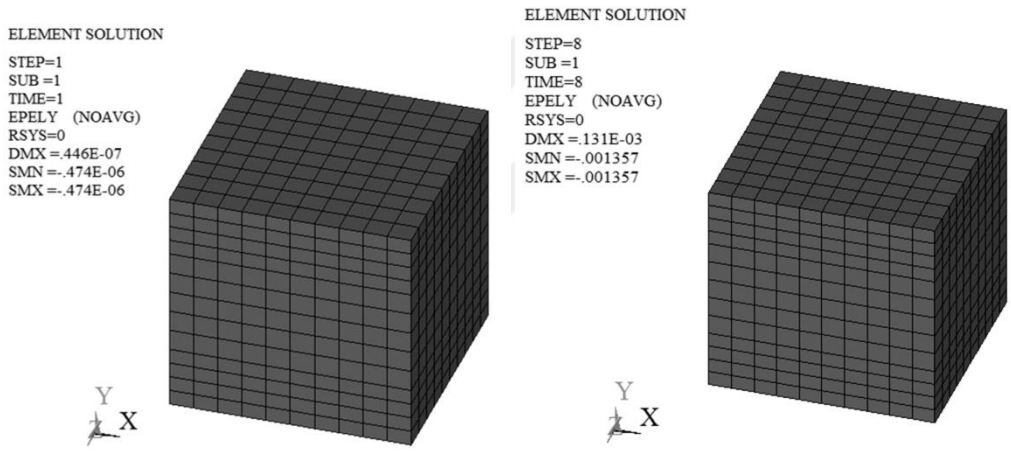

(a) (b)

Figure 3.22 The strain contour plots in Y direction (EPELY) by element solution for (a) the first (0.018 MPa) and (b) the last (51.58 MPa) load steps of FE-2 model

The numerical contour plots of electric field and current density vector sum by element solution for the first (0.018 MPa) and last (51.58 MPa) load steps are compared in Figures 3.23 and 3.24, respectively. The electric field is found to decrease from the lowest to the highest pressure level, while the current density increases. By using Equation 2.6, the electrical resistivity in FE-2 model for the first and last load steps was computed as 356.42 Ωm and 331.38 Ωm, respectively. The electrical resistivity in Specimen 2 for the minimum and maximum pressure loads was respectively equal to 356.43 Ωm and 331.43 Ωm. In this method, the resistivity

decreased by 7% in both the numerical model and experiments. The electrical resistivities obtained from model perfectly matched with experimental results.

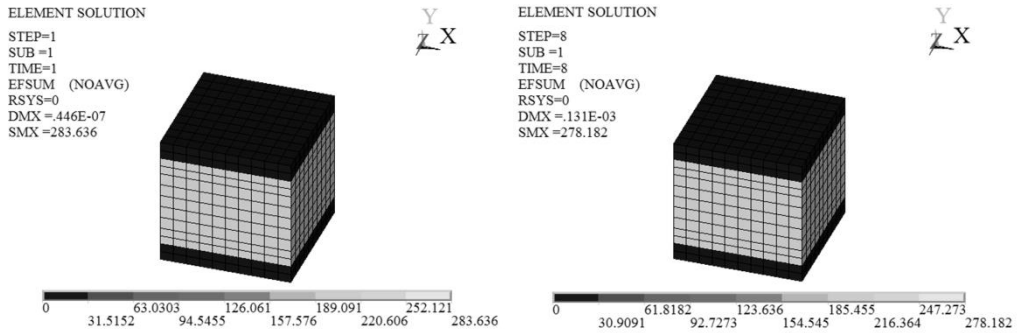

(a) (b)

Figure 3.23 The numerical contour plots of electric field vector sum (EFSUM) by element solution for (a) the first (0.018 MPa) and (b) the last (51.58 MPa) load steps of FE-2 model

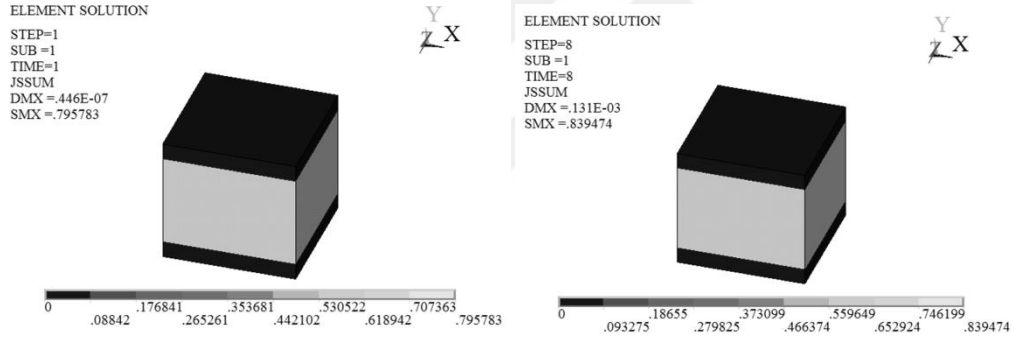

(a) (b)

Figure 3.24 The numerical contour plots of current density vector sum (JSSUM) by element solution for (a) the first (0.018 MPa) and (b) the last (51.58 MPa) load steps of FE-2 model

Figure 3.25 represents the FE results of Specimen 2 plotted with the resistivity change % ρ – strain graph from the experiment, where the electrical resistivity in numerical model is found to decrease with the applied strain, which is also observed in experimental results.

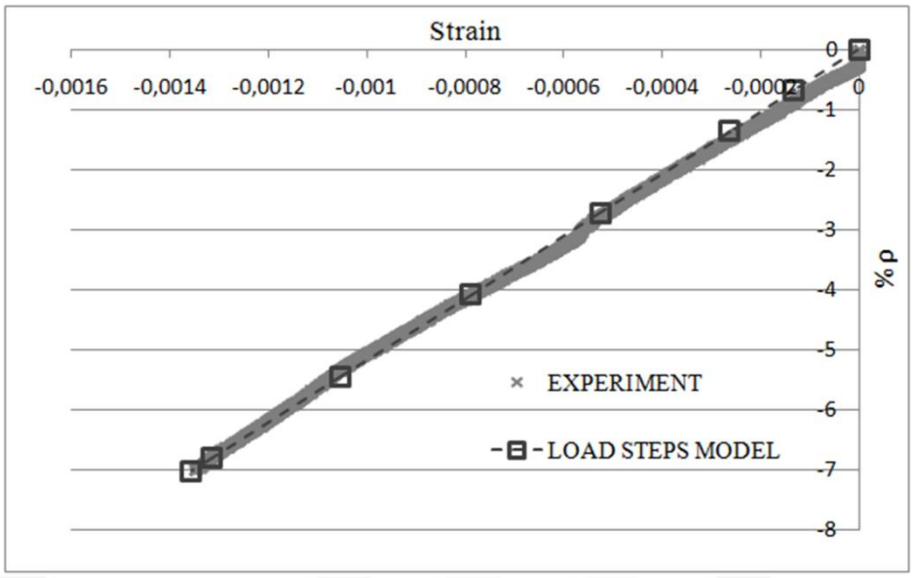

Figure 3.25 Experimental and FEM % ρ – strain graphs using load step method; smart concrete specimen 2 vs FE-2 model

3.2.3 Numerical Results of Finite Element Model FE-3

The stress and strain contour plots by element solution for the first and last load steps are shown in Figures 3.26 and 3.27, respectively. As depicted in Figures 3.26 (a) and (b), the stress in vertical direction is described in terms of a single value, namely, -18000 Pa and -51600000 Pa for the minimum and maximum pressure, respectively. In the same manner, the elastic strain in Y direction is a single value and equals to applied compressive strain (-0.474×10^{-6} and -0.001357), as indicated in Figures 3.27 (a) and (b). The ultimate compressive strain obtained from Specimen 3 (-0.001476) is close to the maximum compressive strain obtained in FE-3 model (-0.001357).

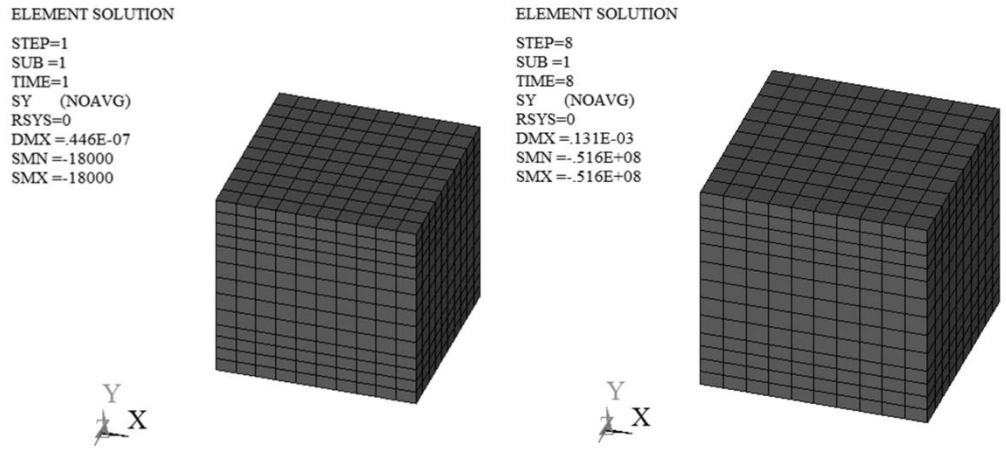

(a) (b)

Figure 3.26 The stress contour plots in Y direction (SY) by element solution for (a) the first (0.018 MPa) and (b) the last (51.58 MPa) load steps of FE-3 model

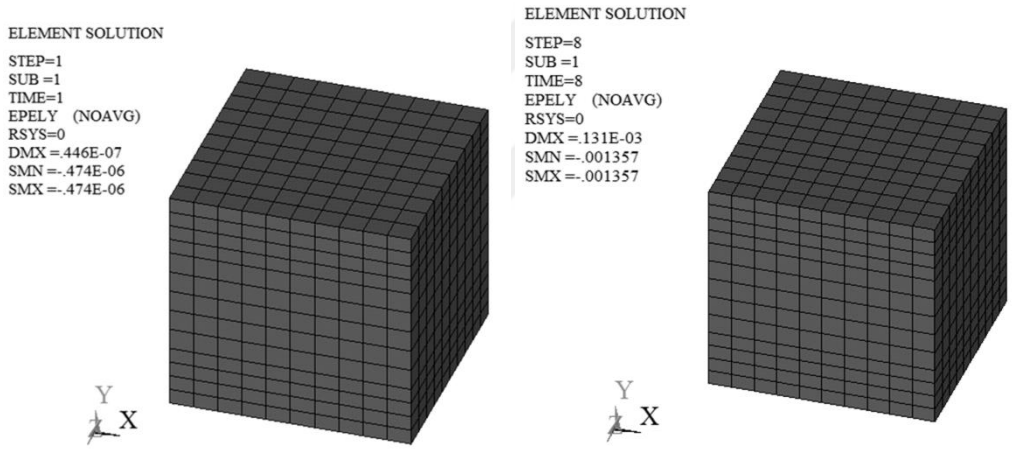

(a) (b)

Figure 3.27 The strain contour plots in Y direction (EPELY) by element solution for (a) the first (0.018 MPa) and (b) the last (51.58 MPa) load steps of FE-3 model

To compare the electric field and current density vector sum by element solution for the first and the last load steps of FE-3 model, contour plots are shown in Figures 3.28 and 3.29, respectively. The electric field decreased from the minimum to the maximum pressure level. On the contrary, the current density increased during analysis. The electrical resistivity in FE-3 model for the first and the last load steps was calculated as 374.36 Ωm and 351.59 Ωm, respectively, by using Equation 2.6. The electrical resistivity in Specimen 3 for the minimum and maximum pressure loads was equal to 374.37 Ωm and 348.93 Ωm, respectively. In this method, the

resistivity decreased by 6% and 6.8% in the numerical model and experiments, respectively. The model results comply with experiments.

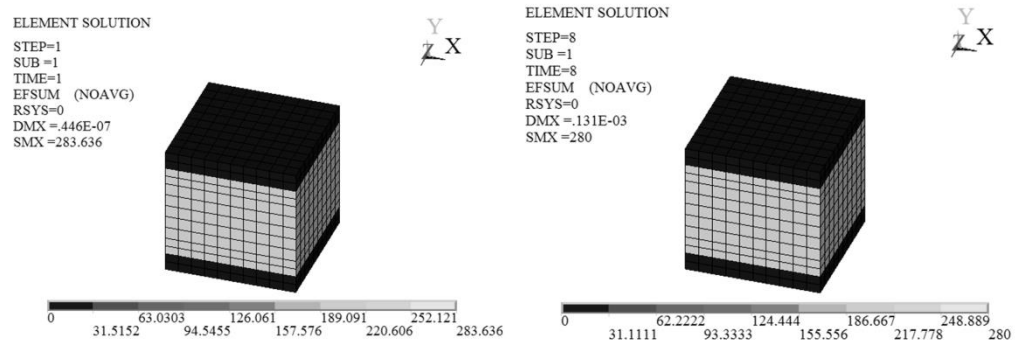

(a) (b)

Figure 3.28 The numerical contour plots of electric field vector sum (EFSUM) by element solution for (a) the first (0.018 MPa) and (b) the last (51.58 MPa) load steps of FE-3 model

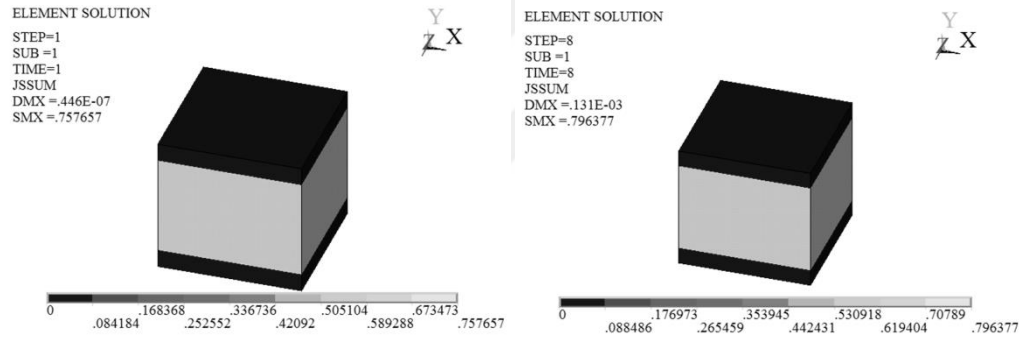

(a) (b)

Figure 3.29 The numerical contour plots of current density vector sum (JSSUM) by element solution for (a) the first (0.018 MPa) and (b) the last (51.58 MPa) load steps of FE-3 model

In Figure 3.30, it was found that there is similarity between experimental and numerical results, for Specimen 3. The electrical resistivity in numerical model decreases with the applied strain, as has been similarly noted for experimental findings.

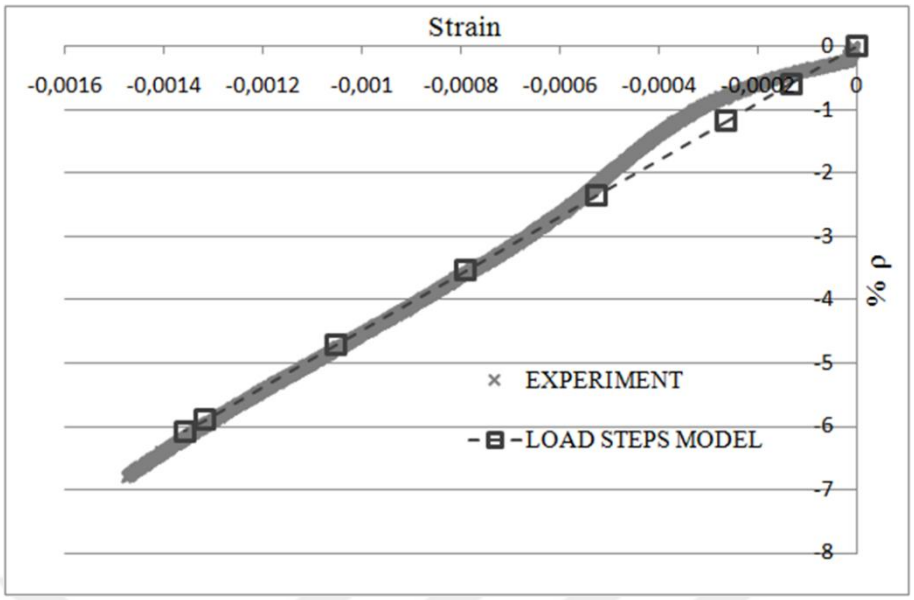

Figure 3.30 Experimental and FEM % ρ – strain graphs using load step method; smart concrete specimen 3 vs FE-3 model

3.3 Numerical Results Using Piecewise Steps Method

In each FE model (FE-1, FE-2 and FE-3), 4 piezoresistive static analyses were performed separately. In each static analysis were defined 3 load steps. The last load step of a static analysis corresponded to the first load step of the subsequent analysis. Time was assigned at the end of each load step, so that the applied loads may vary incrementally over the 3 load steps of the same analysis. In this method, the results gathered from the first load step (0.018 MPa) of the first analysis were compared with the results obtained from the last load step (51.58 MPa) of the last analysis. The electrical resistivity of numerical models was assessed through Equation 2.6. The decrease of electrical resistivity (%) observed in specimens and in FE models using piecewise steps method is summarized in Table 3.3.

Table 3.3 The decrease of electrical resistivity (%) obtained in experimental results and FE models using piecewise steps method

Electrical Resistivity Decrease (%)	FE Model	FE Model Using Equation 2.6 (E/J Model)	Experimental Results
	FE-1	7.1	6.8
	FE-2	7	7
	FE-3	6	6.8

3.3.1 Numerical Results of Finite Element Model FE-1

The numerical stress contour plots by element solution presented in Figures 3.31 (a) and (b) show the vertical stress *SY* as a single value equal to the applied pressure load: -18000 Pa and -51600000 Pa, for the first (0.018 MPa) and the last (51.58 MPa) load steps, respectively. The corresponding strain *EPELY* contour plots are given in Figures 3.32 (a) and (b), where the compressive strain equals to -0.383×10^{-6} and -0.001097, for the first and last load steps, respectively. The ultimate compressive strain obtained from experiment (-0.001057) is consistent with the maximum compressive strain obtained in FE-1 model (-0.001097).

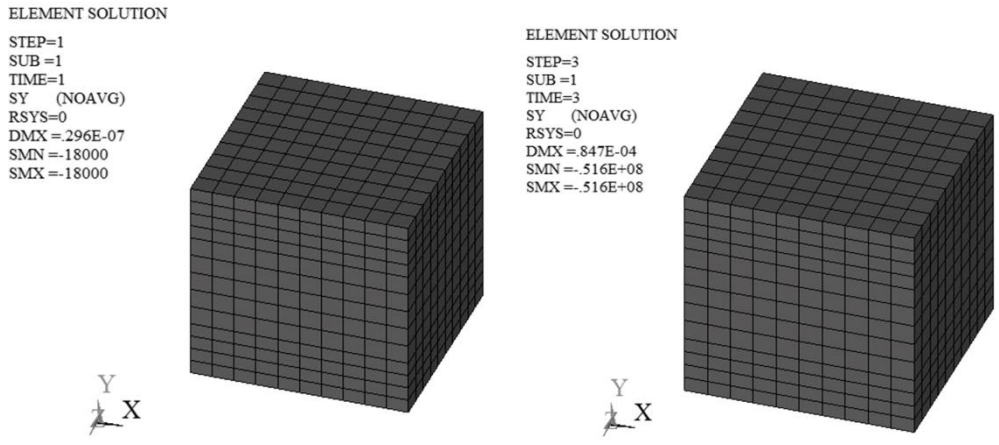

(a) (b)

Figure 3.31 The stress contour plots in Y direction (SY) by element solution for (a) the first (0.018 MPa) and (b) the last (51.58 MPa) load steps of FE-1 model

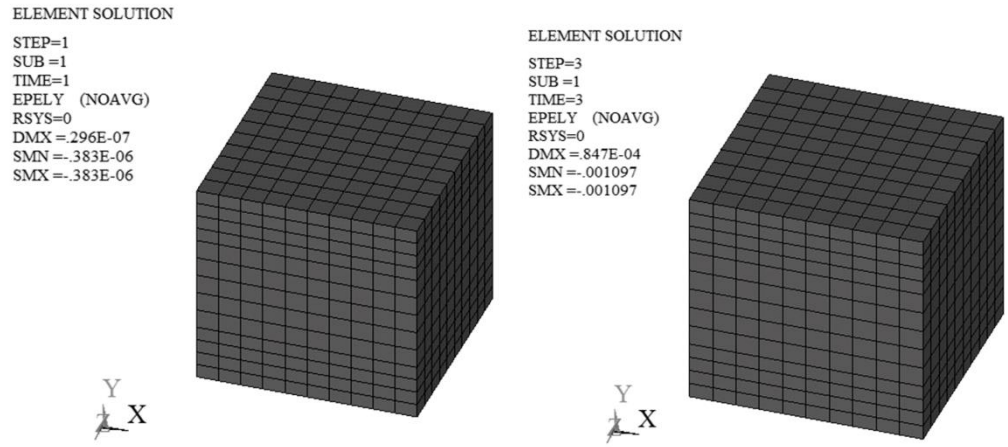

(a) (b)

Figure 3.32 The strain contour plots in Y direction (EPELY) by element solution for (a) the first (0.018 MPa) and (b) the last (51.58 MPa) load steps of FE-1 model

The electric field and current density vector sum by element solution obtained for the first and last load steps are plotted in Figures 3.33 and 3.34, respectively. It is evident that the electric field decreased from the minimum to the maximum stress level, while the current density increased.

In this method, the Equation 2.6 was used to calculate the electrical resistivity of finite element models by dividing the electric field vector sum to the current density vector sum. The electrical resistivity in FE-1 model for the first and last load steps was found equal to 358.66 Ωm and 333.23 Ωm, respectively. The electrical resistivity in Specimen 1 for the minimum and maximum pressure loads was respectively equal to 358.65 Ωm and 334.17 Ωm. The resistivity decreased by 7.1% and 6.8% in the numerical model and experiment, respectively, from the minimum to the maximum loads.

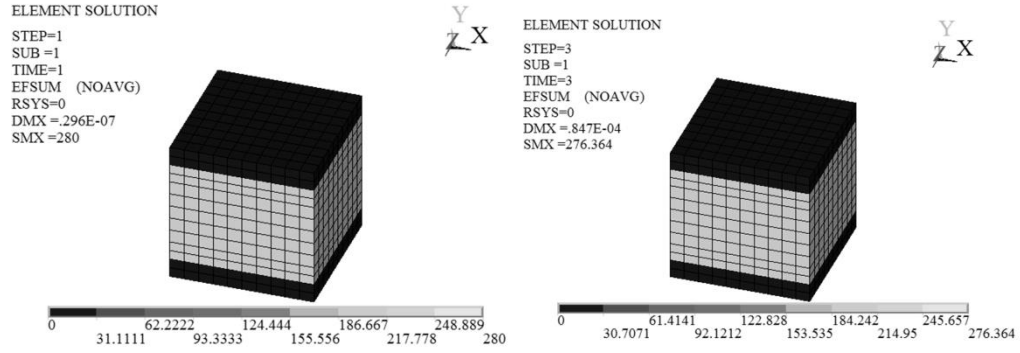

(a) (b)

Figure 3.33 The numerical contour plots of electric field vector sum (EFSUM) by element solution for (a) the first (0.018 MPa) and (b) the last (51.58 MPa) load steps of FE-1 model

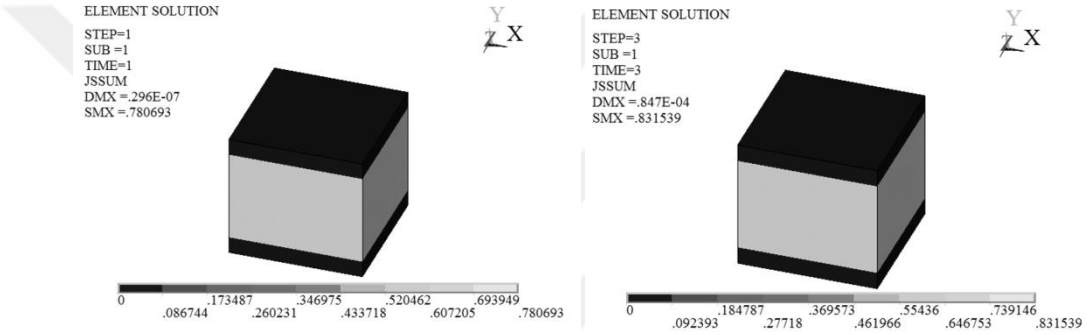

(a) (b)

Figure 3.34 The numerical contour plots of current density vector sum (JSSUM) by element solution for (a) the first (0.018 MPa) and (b) the last (51.58 MPa) load steps of FE-1 model

The electrical resistivity in numerical model decreases with the applied strain, as shown in Figure 3.35. The finite element results obtained from this method are consistent to the experimental results.

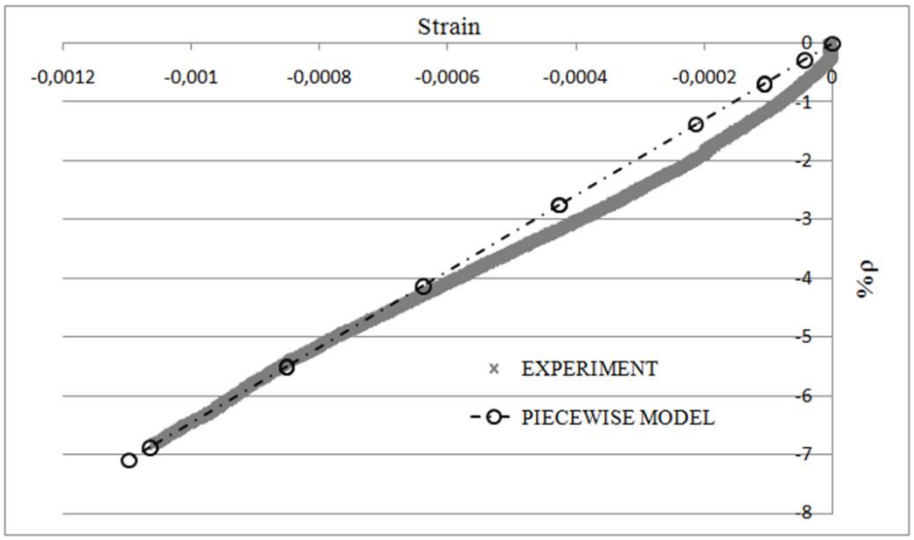

Figure 3.35 Experimental and FEM % ρ – strain graphs using piecewise steps method; smart concrete specimen 1 vs FE-1 model

3.3.2 Numerical Results of Finite Element Model FE-2

Figures 3.36 and 3.37 give ANSYS results for stress and strain at the first and last load steps, respectively. From Figures 3.36 (a) and (b), it can be seen that the stress value in Y direction is equal to the applied minimum and maximum pressure load (-18000 Pa and -51600000 Pa, respectively). Similarly, the elastic strain value in Y direction corresponds to the applied compressive strain (-0.474×10^{-6} and -0.001357) at the same pressure levels, as shown in Figures 3.37 (a) and (b). The ultimate compressive strain obtained from Specimen 2 (-0.001351) and the maximum compressive strain in FE-2 model (-0.001357) are approximately equal.

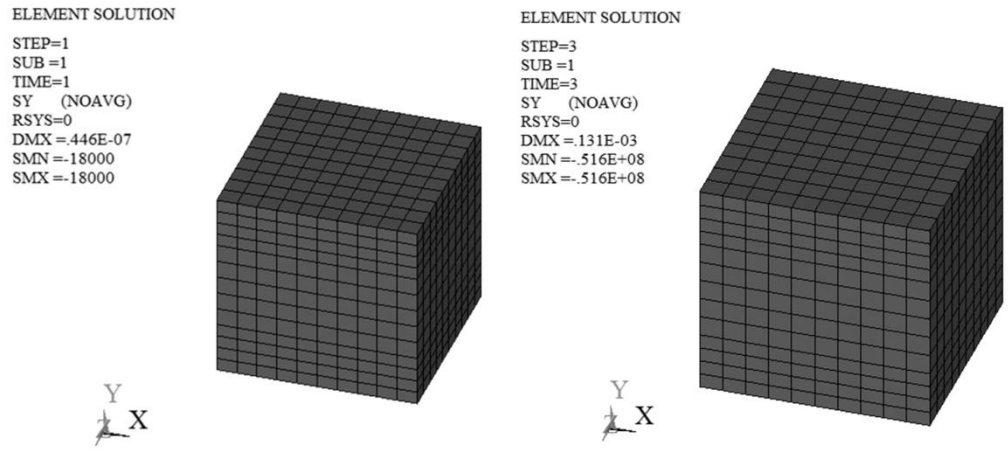

(a) (b)

Figure 3.36 The stress contour plots in Y direction (SY) by element solution for (a) the first (0.018 MPa) and (b) the last (51.58 MPa) load steps of FE-2 model

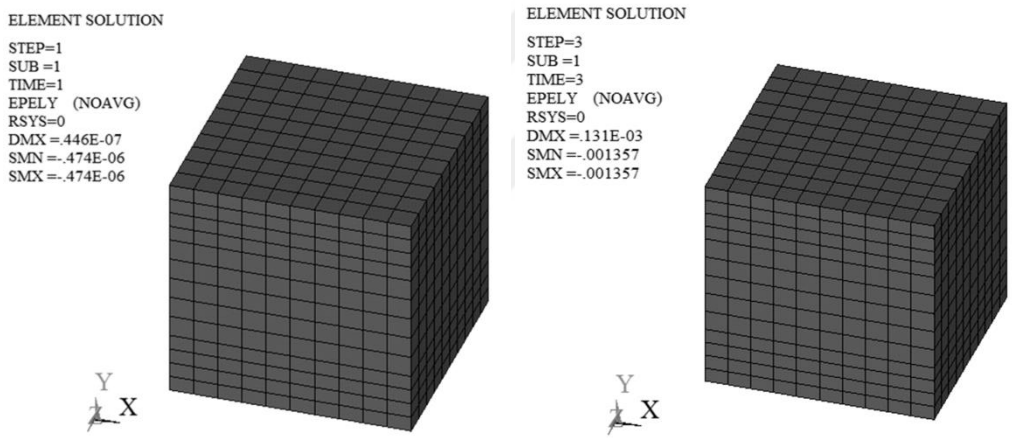

(a) (b)

Figure 3.37 The strain contour plots in Y direction (EPELY) by element solution for (a) the first (0.018 MPa) and (b) the last (51.58 MPa) load steps of FE-2 model

The electric field and current density vector sum by element solution at the first (0.018 MPa) load step are plotted against those obtained at the last (51.58 MPa) load step in Figures 3.38 and 3.39, respectively. The results indicate that there is a decrease in the electric field from the lowest to the highest pressure level, with an increase in current density. Consequently, the resistivity was predicted to decrease in the numerical model, for the first and last load steps, by using Equation 2.6. The simulated electrical resistivity in FE-2 model for the first and last load steps was equal to 356.42 Ωm and 331.38 Ωm, respectively. The electrical resistivity in

Specimen 2 for the minimum and maximum pressure loads was respectively measured as 356.43 Ωm and 331.43 Ωm. The amount of resistivity decrease obtained in numerical model (7%) agree with the experimental results, from minimum to maximum pressure loads.

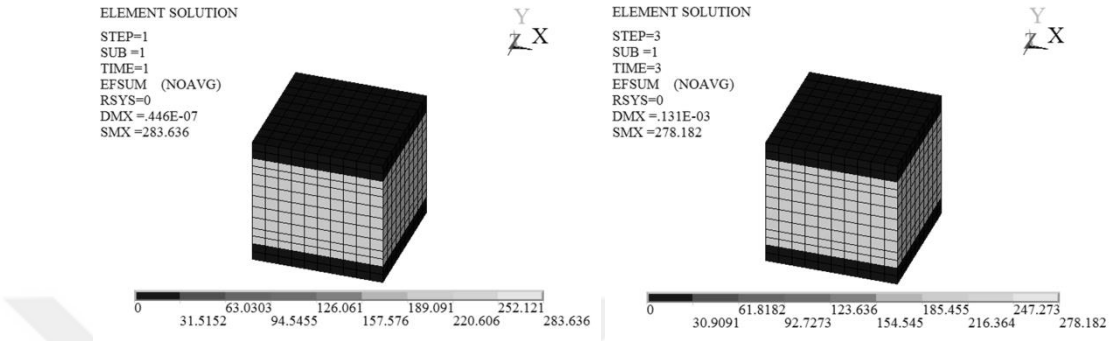

(a) (b)

Figure 3.38 The numerical contour plots of electric field vector sum (EFSUM) by element solution for (a) the first (0.018 MPa) and (b) the last (51.58 MPa) load steps of FE-2 model

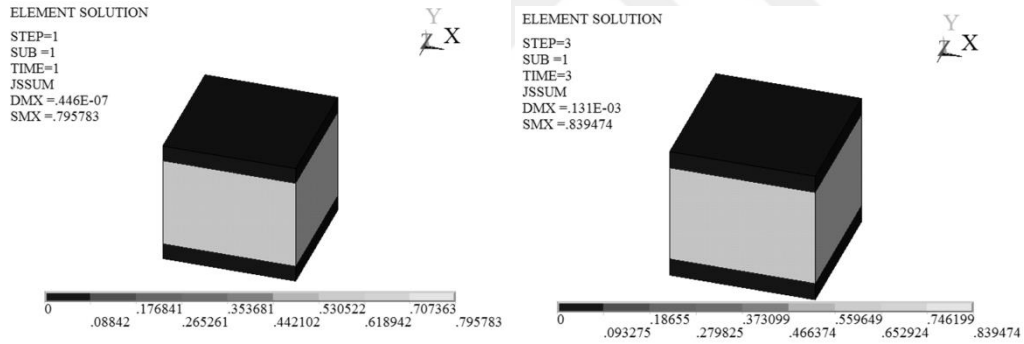

(a) (b)

Figure 3.39 The numerical contour plots of current density vector sum (JSSUM) by element solution for (a) the first (0.018 MPa) and (b) the last (51.58 MPa) load steps of FE-2 model

The results of FE analysis and the resistivity change % ρ - strain graph gathered from the experimental results are plotted in Figure 3.40, which satisfactorily demonstrates the accuracy of FE model of smart concrete. The electrical resistivity in the model decreases with the applied strain, which was also observed in experimental results.

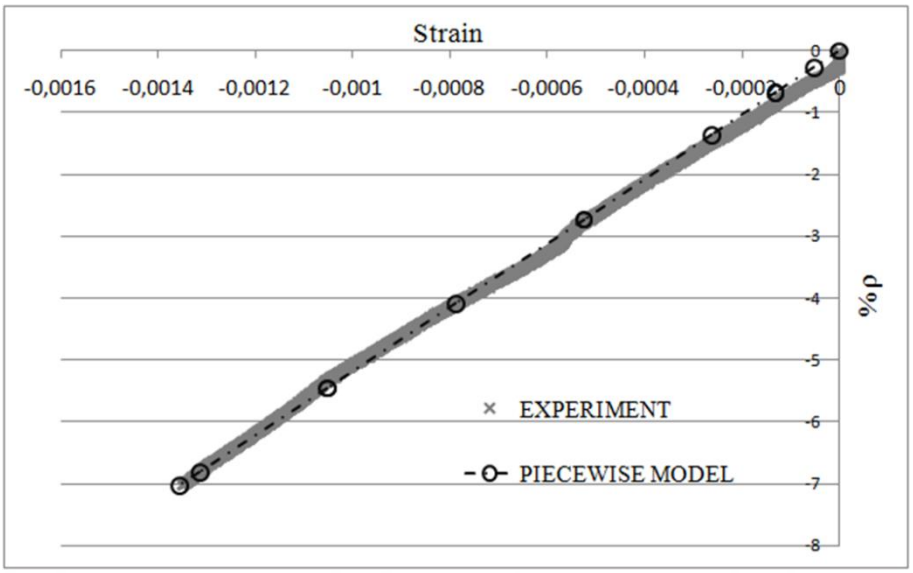

Figure 3.40 Experimental and FEM % ρ – strain graphs using piecewise steps method; smart concrete specimen 2 vs FE-2 model

3.3.3 Numerical Results of Finite Element Model FE-3

Figures 3.41 and 3.42 show the solution output of the proposed model in terms of stress and strain contour plots by element solution for the first and last load steps, respectively. As portrayed in Figures 3.41 (a) and (b), the stress in Y direction (SY) comply with the applied pressure load (-18000 Pa and -51600000 Pa, for the first and last load steps, respectively). In addition, the vertical compressive strain (EPELY) is identical to the applied strain (-0.474×10^{-6} and -0.001357, for the first and last load steps), as indicated in Figures 3.42 (a) and (b). The ultimate compressive strain obtained from Specimen 3 (-0.001476) is comparative to the maximum compressive strain calculated in FE-3 model (-0.001357).

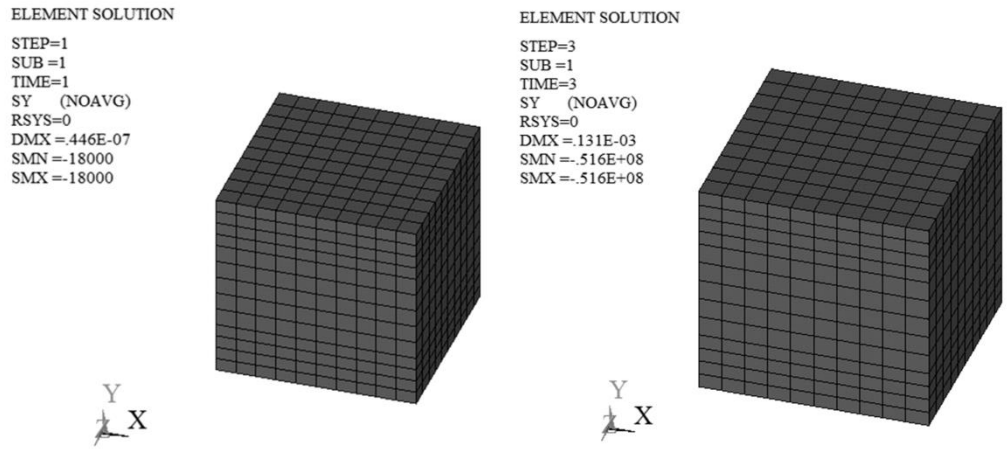

(a) (b)

Figure 3.41 The stress contour plots in Y direction (SY) by element solution for (a) the first (0.018 MPa) and (b) the last (51.58 MPa) load steps of FE-3 model

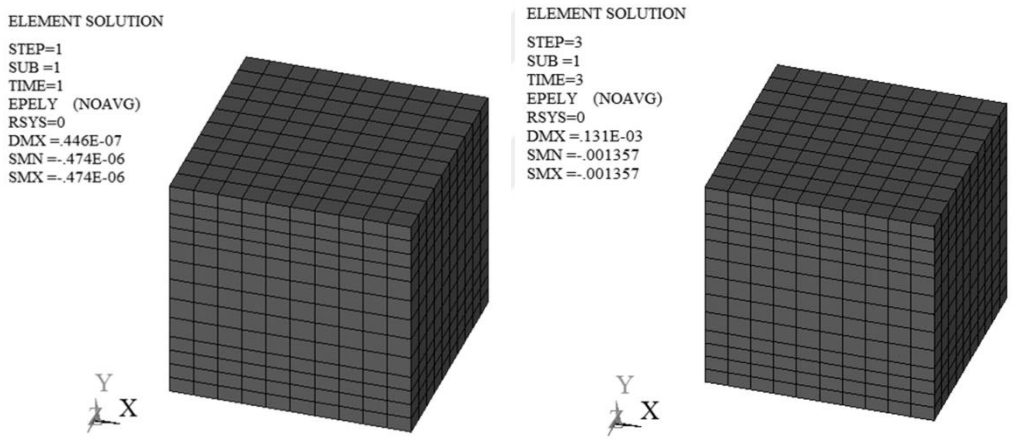

(a) (b)

Figure 3.42 The strain contour plots in Y direction (EPELY) by element solution for (a) the first (0.018 MPa) and (b) the last (51.58 MPa) load steps of FE-3 model

Figures 3.43 and 3.44 show the comparison of the numerical contour plots of electric field and current density vector sum for the first and last load steps, respectively. As the electric field decreased from the minimum to the maximum pressure level, the current density increased. As evident from Equation 2.6, the electrical resistivity was expected to decrease in the model. In FE-3 model, it was evaluated as 374.36 Ωm and 351.59 Ωm at the first and the last load steps, respectively. The electrical resistivity in Specimen 3 for the minimum and maximum pressure loads was respectively measured as 374.37 Ωm and 348.93 Ωm. The

resistivity was lessened by 6% and 6.8% in the numerical and experiments, respectively, from the minimum to the maximum pressure.

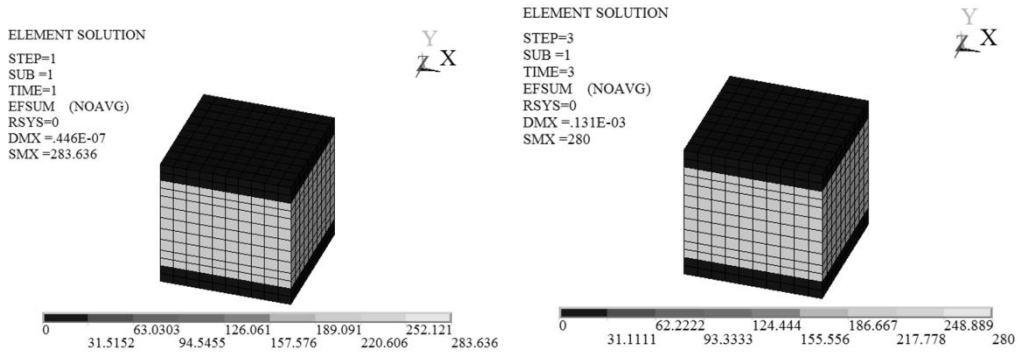

(a) (b)

Figure 3.43 The numerical contour plots of electric field vector sum (EFSUM) by element solution for (a) the first (0.018 MPa) and (b) the last (51.58 MPa) load steps of FE-3 model

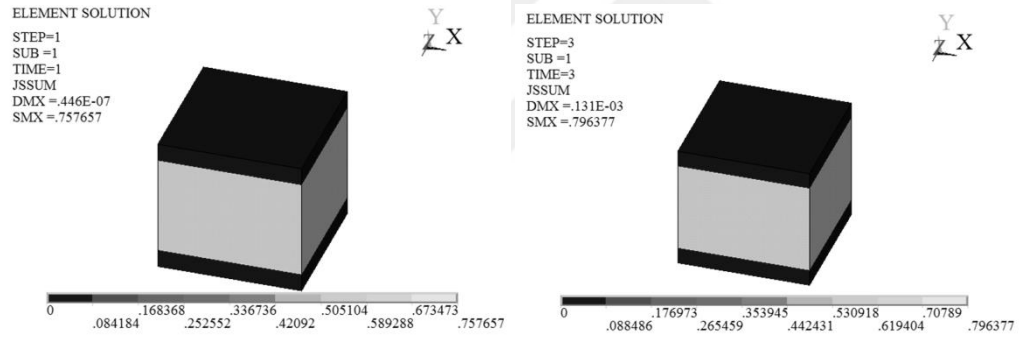

(a) (b)

Figure 3.44 The numerical contour plots of current density vector sum (JSSUM) by element solution for (a) the first (0.018 MPa) and (b) the last (51.58 MPa) load steps of FE-3 model

Electrical resistivity development (% ρ - strain graph) for Specimen 3 is shown in Figure 3.45, and was plotted with the finite element results. The results show that all the curves followed the same trend in which the electrical resistivity decreased with the applied strain.

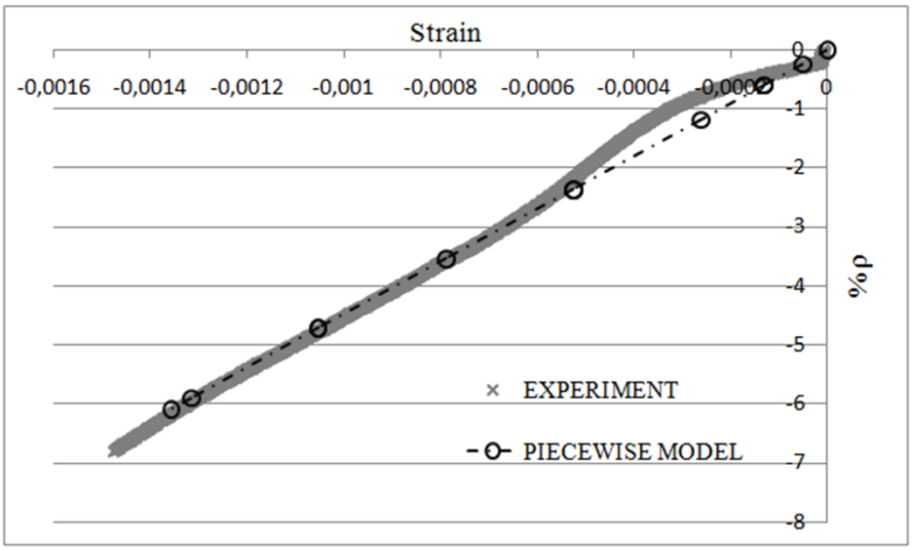

Figure 3.45 Experimental and FEM % ρ – strain graphs using piecewise steps method; smart concrete specimen 3 vs FE-3 model

To compare the finite element results obtained using the numerical methods with the experimental results, Figures 3.46, 3.47 and 3.48 were sketched for the proposed models (FE-1, FE-2 and FE-3 models, respectively). In general, the resistivity change % ρ - strain plots from all the methods agree quite well with the experimental data. For Specimen 1, the finite element results obtained from load steps and piecewise steps methods are closer to experimental results than the finite element results obtained from single step method. This may be due to the use of time-dependent loads in load steps and piecewise steps methods which provides the actual loading environment during test.

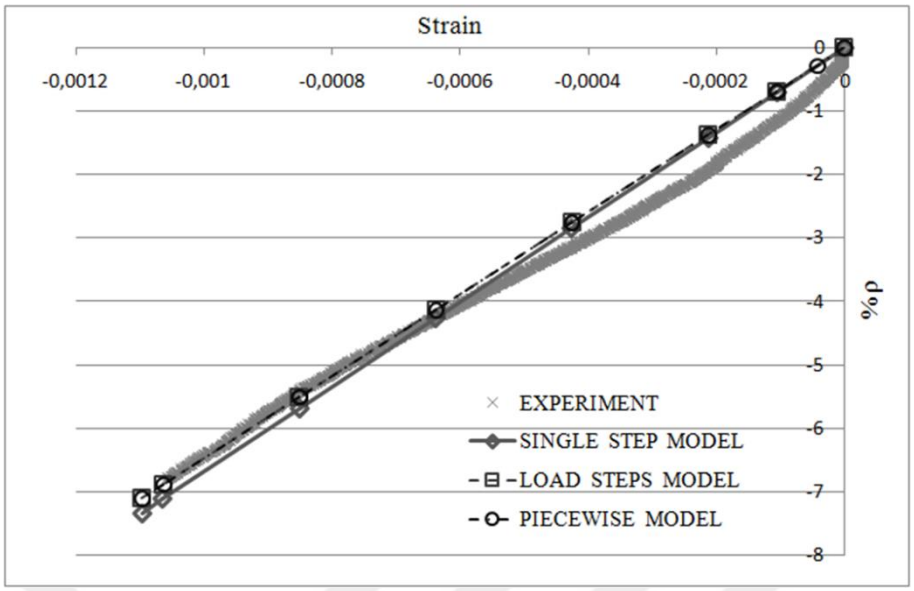

Figure 3.46 Experimental and FEM % ρ – strain graphs using single, load steps and piecewise steps method; smart concrete specimen 1 vs FE-1 model

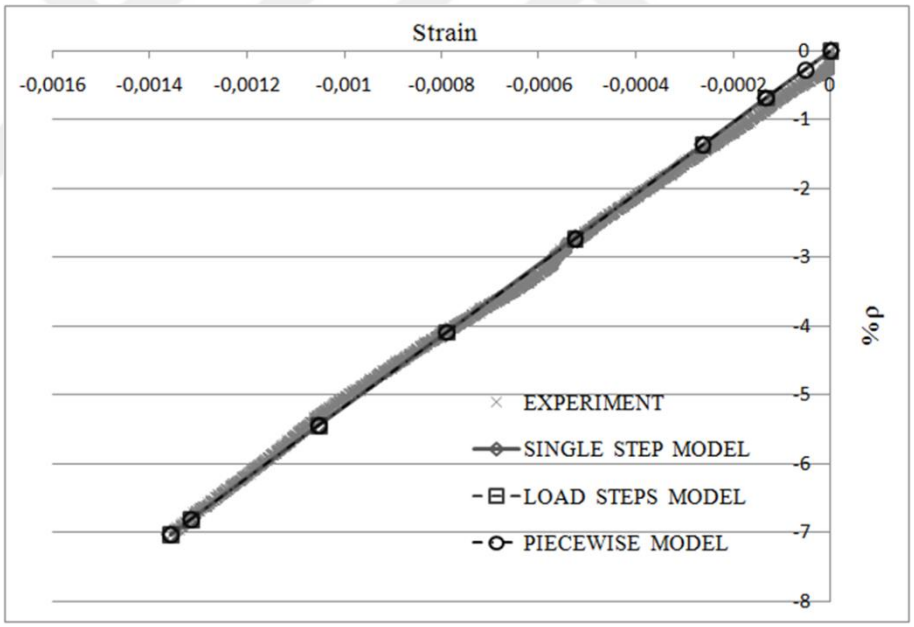

Figure 3.47 Experimental and FEM % ρ – strain graphs using single, load steps and piecewise steps method; smart concrete specimen 2 vs FE-2 model

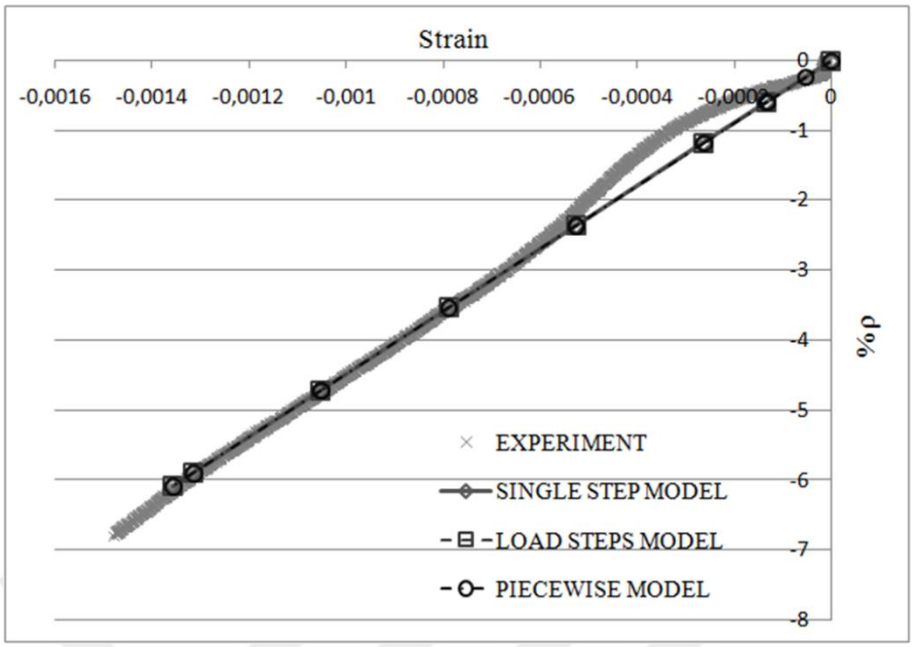

Figure 3.48 Experimental and FEM % ρ – strain graphs using single, load steps and piecewise steps method; smart concrete specimen 3 vs FE-3 model

CHAPTER FOUR
CONCLUSION

The strain-electrical resistivity relation of smart concrete was modeled using ANSYS v. 14.0 program. Piezoresistive static analysis was successfully carried out on three numerical models using finite element method. The finite element models were constructed using twenty-noded solid brick elements SOLID226 to simulate smart concrete specimens. The material properties were taken from experimental data collected from compression test. The smart concrete cube specimens were modeled as volumes with 75×75×75 mm dimensions.

The electrical resistivity was evaluated by following two different ways. In the first way, the electric field and the current density were computed from the model by element solution. The electrical resistivity of numerical models was then calculated by dividing the electric field vector sum to the current density vector sum. In the second way, the electric potential difference and the current were determined from the model and the electrical resistance was calculated using Ohm's law. Here, the electrical resistivity of FE models was calculated by taking into account the length and cross sectional area of the model.

Finite element solution was evaluated through three different methods. Single step method was used to separately apply 8 static pressure loads on finite element models in 8 static analyses. Load steps method helped to apply 8 time-dependent loads in a single static analysis. The loads were assumed to vary slowly with respect to time. Piecewise steps method served to conduct 4 static analyses with 3 time-dependent loads in each analysis. The numerical contour plots of stress, strain, electric field and current density by element solution for the lowest and highest pressure level obtained from the three methods were examined and discussed. The voltage and current read from the program were compared to experimental findings. The electrical resistivity change % ρ – strain graph obtained from finite element analysis was compared to the experimental graph. The information and results gathered within the scope of this thesis are as follow.

1. The simulation of smart concrete by finite element method was successfully conducted in this study.

2. The maximum compressive strain obtained in all finite element models was very close to the ultimate compressive strain obtained from experiments, regardless of the method used during solution.

3. The electrical resistivity of the finite element models decreased from the lowest to the highest pressure load, regardless of the method used during solution. The decrease of electrical resistivity was also observed in experiments. The compressive strain decreased the electrical resistivity with closure of microvoids, resulting in increase of fiber-matrix and fiber-fiber contact.

4. The electric field decreased from the minimum to the maximum pressure load, while the current density increased, regardless of the method used during solution. The potential difference decreased from the lowest to the highest pressure level, while the electric current increased, regardless of the method used during solution. The decrease of electrical potential difference and increase of electric current was also observed in experiments.

5. Similar results were obtained from the evaluation of electrical resistivity through the use of electric field and current density and the use of Ohm's law. In addition, finite element results gathered using different numerical methods were very close to the piezoresistive behavior measured during experimental work.

The similarity between finite element results and experimental findings indicates that the proposed numerical model is able to predict the piezoresistive behavior of smart concrete. Modeling of smart concrete will enable the creation of reliable finite element models that can be used by structural engineers to predict the strain-sensing capability of smart concrete for structural health monitoring.

REFERENCES

ANSYS, (2011). *ANSYS help system, coupled-field analysis guide*, ANSYS, Inc. Retrieved October 2011, from https://www.sharcnet.ca/Software/Ansys/14.0/en-us/help/ans_cou/Hlp_G_COU3_piezores.html.

Azhari, F., & Banthia, N. (2012). Cement-based sensors with carbon fibers and carbon nanotubes for piezoresistive sensing. *Cement and Concrete Composites, 34* (7), 866-873.

Chen, P. W., & Chung, D. D. L. (1993). Carbon fiber reinforced concrete as a smart material capable of non-destructive flaw detection. *Smart Materials and Structures, 2* (1), 22-30.

Chowdhury, S. (2017). *Experimental investigations and modeling of the strain sensing response of matrices containing metallic inclusions*. Master of Science Thesis, Arizona State University, Arizona.

Chung, D. D. L. (1998). Self-monitoring structural materials. *Materials Science and Engineering R: Reports, 22* (2), 57-78.

Chung, D. D. L. (2001). Review functional properties of cement–matrix composites. *Journal of Material Science, 36* (6), 1315-1324.

Chung, D. D. L. (2002). Piezoresistive cement-based materials for strain sensing. *Journal of Intelligent Material Systems and Structure, 13* (9), 599-609.

Chung, D. D. L. (2010). Electrical properties of composite materials. In *Composite materials: science and applications* (2nd ed.) (203-275). New York: Springer.

Fu, X., & Chung, D. D. L. (1997). Effect of curing age on the self-monitoring behavior of carbon fiber reinforced mortar. *Cement and Concrete Research, 27* (9), 1313-1318.

Fu, X., Chung, D. D. L., Ma, E., & Anderson, W. A. (1997). Self-monitoring in carbon fiber reinforced mortar by reactance measurement. *Cement and Concrete Research, 27* (6), 845-852.

García-Macías, E., D'Alessandro, A., Castro-Triguero, R., Pérez-Mira, D., & Ubertini, F. (2017). Micromechanics modeling of the electrical conductivity of carbon nanotube cement-matrix composites. *Composites Part B: Engineering, 108,* 451-469.

Islam, M. M., Khatun, M. S., Islam, M. R. U., Dola, J. F., Hussan, M., & Siddique, A. (2014). Finite element analysis of steel fiber reinforced concrete (SFRC): validation of experimental shear capacities of beams. *10th International Conference on Mechanical Engineering, ICME 2013, Procedia Engineering, 90,* 89-95.

Madenci, E., & Güven I. (2006). *The finite element method and applications in engineering using ANSYS* (1st ed.). New York: Springer.

Mason, W. P. & Thurston, R. N. (1957). Use of piezoresistive materials in the measurement of displacement, force, and torque. *Journal of the Acoustical Society of America, 29,* 1096-1101.

Mohammed, A. A. S., Moussa, W. A., & Lou, E. (2008). High sensitivity MEMS strain sensor: design and simulation. *Sensors, 8* (4), 2642-2661.

Teomete, E. (2014). Transverse strain sensitivity of steel fiber reinforced cement composites tested by compression and split tensile tests. *Construction and Building Materials, 55,* 136-145.

Teomete, E. (2017). *Akıllı beton üretimi*. TUBITAK araştırma raporu, Izmir.

Teomete, E., & Erdem, T. K. (2011). Cement based strain sensor: a step to smart concrete. *Cement, Wapno, Beton, 2* , 78-91.

Teomete, E., & Koçyiğit, O. I. (2013). Tensile strain sensitivity of steel fiber reinforced cement matrix composites tested by split tensile test. *Construction and Building Materials, 47*, 962-968.

Teomete, E., & Koçyiğit, O. I. (2015). Correlation between compressive strain and electrical resistance in carbon fiber reinforced cement composites. *Cement, Wapno, Beton, 1*, 1-10.

Wen, S., & Chung, D. D. L. (2000). Uniaxial tension in carbon fiber reinforced cement, sensed by electrical resistivity measurement in longitudinal and transverse directions. *Cement and Concrete Research, 30* (8), 1289-1294.

Wen, S., & Chung, D. D. L. (2006). Model of piezoresistivity in carbon fiber cement, *Cement and Concrete Research, 36* (10), 1879-1885.

Xiao, H., Li H., & Ou, J. (2010). Modeling of piezoresistivity of carbon black filled cement-based composites under multi-axial strain. *Sensors and Actuators: A. Physical, 160* (1), 87-93.